

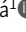










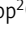



ARTICLE

Segmented filamentous bacteria-induced epithelial MHCII regulates cognate CD4⁺ IELs and epithelial turnover

Tomáš Brabec^{1,2}, Martin Schwarzer³, Katarína Kováčová¹, Martina Dobešová^{1,2}, Dagmar Schierová⁴, Jiří Březina², Iva Pacáková¹, Dagmar Šrůtková³, Osher Ben-Nun⁵, Yael Goldfarb⁵, Iva Šplíchalová², Michal Kolář⁶, Jakub Abramson⁵, Dominik Filipp², and Jan Dobeš¹

Intestinal epithelial cells have the capacity to upregulate MHCII molecules in response to certain epithelial-adhesive microbes, such as segmented filamentous bacteria (SFB). However, the mechanism regulating MHCII expression as well as the impact of epithelial MHCII-mediated antigen presentation on T cell responses targeting those microbes remains elusive. Here, we identify the cellular network that regulates MHCII expression on the intestinal epithelium in response to SFB. Since MHCII on the intestinal epithelium is dispensable for SFB-induced Th17 response, we explored other CD4⁺ T cell-based responses induced by SFB. We found that SFB drive the conversion of cognate CD4⁺ T cells to granzyme⁺ CD8α⁺ intraepithelial lymphocytes. These cells accumulate in small intestinal intraepithelial space in response to SFB. Yet, their accumulation is abrogated by the ablation of MHCII on the intestinal epithelium. Finally, we show that this mechanism is indispensable for the SFB-driven increase in the turnover of epithelial cells in the ileum. This study identifies a previously uncharacterized immune response to SFB, which is dependent on the epithelial MHCII function.

Introduction

Intestinal epithelial cells (IECs) form a single-layered intestinal epithelium, which facilitates the absorption of nutrients and water and is critical for restraining the intestinal microbiota and pathogens in the gut lumen. Loss of intestinal epithelium barrier integrity leads to the translocation of luminal components to the surrounding tissue and may result in the development of severe inflammatory intestinal disorders due to the breakdown of intestinal homeostasis (Bevins and Salzman, 2011; Maloy and Powrie, 2011).

It has been recognized for a long time that IECs can express the major histocompatibility complex class II (MHCII) molecules (Arnaud-Battandier et al., 1986; Gorvel et al., 1984; Scott et al., 1980). More recently, MHCII⁺ IECs were suggested to function as non-classical antigen-presenting cells (APCs), which can modulate the severity of intestinal pathologies, such as induced colitis in mice (Jamwal et al., 2020), graft-versus-host disease (Koyama et al., 2019), or intestinal tumorigenesis (Beyaz et al.,

2021). This suggests that the IEC-dependent presentation of antigens in the MHCII context may contribute to CD4⁺ T cell-mediated adaptive immune responses. Additional studies revealed that the MHCII expression on IECs is partially regulated by the circadian clock and dietary intake rhythmicity (Tuganbaev et al., 2020), as well as by diet composition (Beyaz et al., 2021). Moreover, the MHCII expression on intestinal stem cells was implicated in organizing the stem cell differentiation potential to distinct epithelial cell lineages, yet the mechanism remained elusive (Biton et al., 2018). In spite of this progress, the functional significance of MHCII⁺ IECs under steady-state conditions is still poorly understood, especially with regard to its impact on shaping T cell responses to microbes responsible for MHCII induction on IECs.

The majority of luminal microbiota is prevented from direct adhesion to the apical side of IECs by the mucus layer, which also contains a gradient of IgA antibodies of different specificities

¹Department of Cell Biology, Faculty of Science, Charles University, Prague, Czech Republic; ²Laboratory of Immunobiology, Institute of Molecular Genetics of the Czech Academy of Sciences, Prague, Czech Republic; ³Laboratory of Gnotobiology, Institute of Microbiology of the Czech Academy of Sciences, Nový Hrádek, Czech Republic; ⁴Laboratory of Anaerobic Microbiology, Institute of Animal Physiology and Genetics of the Czech Academy of Sciences, Prague, Czech Republic; ⁵Department of Immunology and Regenerative Biology, Weizmann Institute of Science, Rehovot, Israel; ⁶Laboratory of Genomics and Bioinformatics, Institute of Molecular Genetics of the Czech Academy of Sciences, Prague, Czech Republic.

Correspondence to Jan Dobeš: jan.dobes@natur.cuni.cz; Dominik Filipp: dominik.filipp@img.cas.cz.

© 2023 Brabec et al. This article is distributed under the terms of an Attribution-Noncommercial-Share Alike-No Mirror Sites license for the first six months after the publication date (see <http://www.rupress.org/terms/>). After six months it is available under a Creative Commons License (Attribution-Noncommercial-Share Alike 4.0 International license, as described at <https://creativecommons.org/licenses/by-nc-sa/4.0/>).

and various antimicrobial peptides. However, a small fraction of intestinal microbes is not physically segregated from IECs but instead physically interact with them (Blumershine and Savage, 1977; Farkas et al., 2015; Klaasen et al., 1992). One of the best-characterized members of this category is segmented filamentous bacteria (SFB, proposed name *Candidatus savagella*) (Thompson et al., 2012)—anaerobic, spore-forming, clostridia-like microorganisms, which live in close association with IECs (Ivanov and Littman, 2010). To facilitate their interaction with IECs, SFB use hook-like protrusions poked out inside IECs. Through this unique infection strategy, most of the SFB cell remains extracellular and only a smaller part infects the inner intracellular space of the IECs without disrupting their plasma membrane (Ladinsky et al., 2019). Interestingly, endocytic vesicles containing SFB cell wall-associated proteins are shed into the cytosol from the tip of the SFB-hook in the actin-dependent endocytic manner and shuttled through the endosomal-lysosomal compartment of IECs (Ladinsky et al., 2019), where MHCII presentation machinery is canonically present. Tight adhesion of SFB to IECs induces a strong immune response in the intestine, which is characterized by the accumulation of T helper 17 (T_H17) cells (Atarashi et al., 2015; Gaboriau-Routhiau et al., 2009; Ivanov et al., 2009; Yang et al., 2014) and increased production of IL-17 and IL-22, as well as by increased production of IgA by plasma cells (Lecuyer et al., 2014). These responses in turn limit the overgrowth of SFB (Kumar et al., 2016; Shih et al., 2014; Suzuki et al., 2004). Interestingly, while SFB are able to induce MHCII expression in IECs (Goto et al., 2014; Tuganbaev et al., 2020; Umesaki et al., 1995), IECs' MHCII-mediated antigen presentation is dispensable for SFB-driven Th17 response (Goto et al., 2014) and so far, no function with regard to SFB-driven T cell responses was attributed to it.

IECs are wired to the immune system through close physical and functional interactions with various immune cells located in the intraepithelial space of the gut. These, in particular, include intraepithelial lymphocytes (IELs) (Cheroutre et al., 2011; Hayday et al., 2001), a heterogeneous group of T cells implicated in immune protection against various intestinal pathogens including viruses (Masopust et al., 2006; Müller et al., 2000; Shires et al., 2001), bacteria (Mombaerts et al., 1993), or parasites (Chardès et al., 1994; Lepage et al., 1998). Since IELs reside in epithelial tissue, they are characterized by high expression of an adhesion integrin molecule CD103, which facilitates their interaction with IECs through its binding to E-cadherin (Cepek et al., 1994; Kilshaw and Murant, 1990). While IELs can express either $\alpha\beta$ or $\gamma\delta$ T cell receptors (TCR), a large fraction of IELs expresses CD8 $\alpha\alpha$ homodimers, which serve as ligands for epithelium-expressed thymus leukemia antigen (TLA, encoded by the *H2-T3* gene) (Leishman et al., 2001). Based on their origin, IELs are classified into two major subtypes—natural IELs and induced IELs (iIELs). While natural IELs are generated directly in the thymus and migrate to effector tissue, iIELs in contrast arise from activated, antigen-experienced conventional $\alpha\beta$ TCR⁺ T cells (Cheroutre et al., 2011). iIEL arising from CD4⁺ T cells lose their classical ThPOK-guarded CD4⁺ identity upon specific stimulus through the induction of Runx3 expression, which

counteracts ThPOK (Reis et al., 2013). The Runx3-mediated demise of ThPOK expression (Mucida et al., 2013) eventually results in the establishment of a potent CD8⁺ T cell-like phenotype manifested by large cytolytic granules (Shires et al., 2001). This elegant mechanism allows antigen-specific T cells to lose their CD4⁺ T helper phenotype to become cytotoxic iIELs while maintaining MHCII restriction (He et al., 2005; Mucida et al., 2013). Nevertheless, the role of MHCII-restricted iIELs under homeostatic conditions, as well as the mechanisms that drive their development, are only beginning to be explored.

Here, we report that intestinal colonization by SFB promotes conversion of SFB-specific CD4⁺ T cells into granzyme-expressing iIEL and their accumulation in the gut intraepithelial space in a manner dependent on epithelial MHCII expression. Moreover, our data provide critical insights into the physiological role of these converted cytotoxic iIELs by demonstrating their ability to regulate the IECs turnover.

Results

SFB induce strong MHCII expression in IECs

The hallmark of the immune response to SFB colonization is the upregulation of MHCII by IECs (Goto et al., 2014; Tuganbaev et al., 2020; Umesaki et al., 1995), yet the immune factors induced by SFB regulating MHCII expression on IECs are unknown. First, we decided to validate the ability of SFB to induce MHCII on IECs in the SFB-free mice acquired from the Jackson Laboratory (JAX) (Ivanov et al., 2009) colonized by SFB at weaning on top of their standard microbiota 2 as well as 9 wk after colonization (Fig. 1, A and B; and Fig. S1, A and B) and also in SFB-colonized germ-free (GF) animals (Fig. 1 C).

Next, we focused on immune signals utilized to regulate the MHCII expression on IECs in response to SFB colonization. While SFB are well known for their ability to induce the T_H17 response with signature cytokines IL-17 and IL-22 (Gaboriau-Routhiau et al., 2009; Ivanov et al., 2009), it was also reported that SFB can increase IFN γ production in the gut (Gaboriau-Routhiau et al., 2009). The latter finding might be crucial since IFN γ is a well-documented modulator of MHCII expression (Koyama et al., 2019; Thelemann et al., 2014; Van Der Kraak et al., 2021). Therefore, we next measured the induction of IL-17A and IFN γ cytokines in the small intestinal (SI) lamina propria (SI-LP) after SFB colonization of JAX mice and found that both of those cytokines are induced by SFB colonization (Fig. 1 D and Fig. S1 C).

To test whether SFB-induced IFN γ or IL-17A cytokine production affects MHCII expression on IECs, we blocked the effector function of these two cytokines in SFB-colonized WT mice by specific neutralizing antibodies. Strikingly, while IFN γ blockade completely abrogated MHCII expression on IECs, the blockade of IL-17A led to a two-fold increase in the frequency of MHCII⁺ IECs (Fig. 1 E). Since a recent study reported that during the weaning period (3 wk of age) mice show strong but transient production of IFN γ (Al Nabhani et al., 2019), we wondered whether blockade of this transient IFN γ stimulus associated with weaning could affect the MHCII expression on IECs later in life. To this end, we injected WT SFB⁺ mice with IFN γ blocking antibody

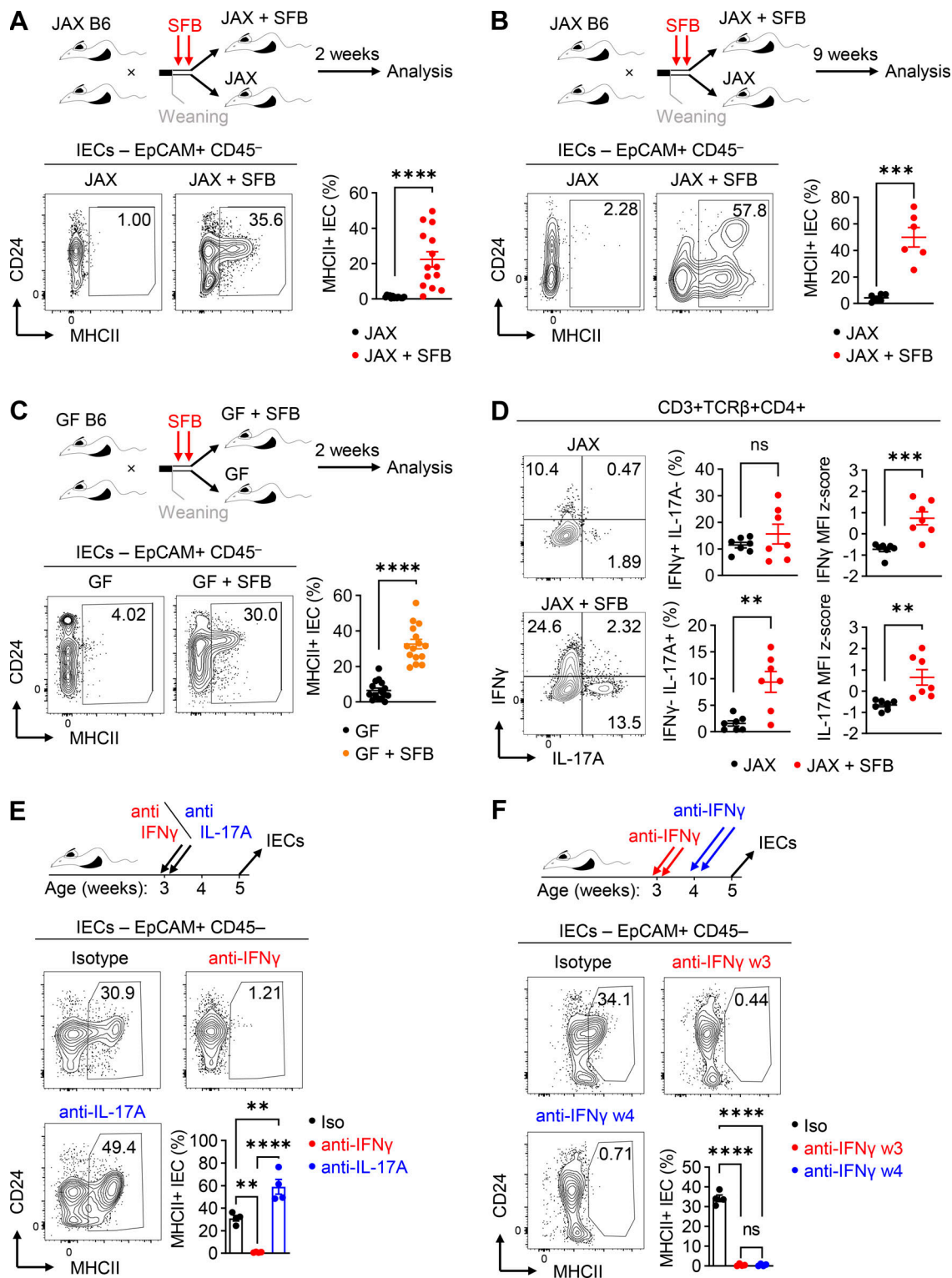


Figure 1. **SFB drive MHCII expression on the intestinal epithelium through induction of IFN γ .** (A) FACS analysis of SI-IECs isolated from 5-wk-old WT animals carrying microbiota from the Jackson Laboratory (JAX), half of which were colonized with SFB at 21 and 22 days of age (JAX + SFB). FACS plots on the left show representative gating. The plot on the right shows an overview of the results and statistical analysis. Five independent experiments, $n = 15$. (B) FACS analysis of SI-IECs isolated from 12-wk-old WT animals carrying microbiota from the Jackson Laboratory (JAX), half of which were colonized with SFB at 21 and 22 days of age (JAX + SFB). FACS plots on the left show representative gating. Plot on the right shows an overview of the results and statistical analysis. Two independent experiments, $n = 6$. (C) FACS analysis of SI-IECs isolated from 5-wk-old GF WT animals, half of which were colonized with SFB at 21 and 22 days of age (GF + SFB). FACS plots on the left show representative gating. The plot on the right shows an overview of the results and statistical analysis. Five independent experiments, $n = 15$. (D) FACS analysis of IFN γ and IL-17a production by CD3⁺ TCR β ⁺ CD4⁺ T cells in SI-LP of JAX and JAX + SFB mice. Plots on the left show representative gating. Plots on the right show quantification of frequencies of IFN γ ⁺ IL-17a⁻ and IFN γ ⁺ IL-17a⁺ and batch normalized mean

fluorescence intensity (MFI) of IFN γ and IL-17a in all CD45⁺ TCR β ⁺ CD4⁺ T cells. Two independent experiments, $n = 7$. **(E)** Flow cytometry analysis of MHCII expression on SI-IECs in SFB-colonized mice, which were i.p. treated with either IL-17a or IFN γ -neutralizing antibodies or isotype control at 21 and 22 days of age, 250 μ g in 100 μ l of PBS in each injection. Plots show representative gating and the statistical overview of the data. Two independent experiments, $n = 4$. **(F)** WT mice derived from SFB-colonized parents were i.p. treated either with isotype antibody or with IFN γ -neutralizing antibody at either 21 and 22 days or at 28 and 29 days of age, 250 μ g in 100 μ l of PBS in each injection. Plots show representative gating and a statistical overview of the data. Two independent experiments, $n = 4$. Data in A–C were tested by Student's t test. Data in D and E were tested by ordinary one-way ANOVA with Holm–Šidák's multiple comparisons test. ns, not significant; **, $P < 0.01$; ***, $P < 0.001$; ****, $P < 0.0001$. Numbers beside gates represent frequencies from parent population or MFI (C). Horizontal lines and bars show mean \pm SEM.

either at 3 or at 4 wk of age and analyzed them at the age of 5 wk. In both cases, the MHCII expression on IECs was completely blocked (Fig. 1 F). Thus, continuous IFN γ production seems to be indispensable for the expression of MHCII on IECs not only during but also after the weaning period.

MHCII expression on IEC is induced by T cell–derived IFN γ in a cDC1-dependent manner

Next, we sought to identify the cellular source of IFN γ responsible for the induction of MHCII expression on IECs. We utilized single-cell RNA sequencing (scRNA-seq) analysis of SI-LP from JAX mice and their littermates colonized by SFB (Fig. 2, A–F). We identified several major leukocyte populations including B cells, plasma cells, several types of myeloid cells, and innate lymphoid cells (ILC2 and ILC3 cells), as well as a cluster containing other lymphoid cells by clustering analysis (Fig. 2, A and C, left panels). Further analysis of the mixed lymphoid cluster revealed several subclusters corresponding to natural killer (NK) cells, NK T (NKT) cells, both naïve and mature $\gamma\delta$ T cells, naïve and mature CD8⁺ $\alpha\beta$ T cells, CD4⁺ naïve T cells, regulatory T cells (Tregs), and conventional CD4⁺ T cells (Fig. 2, A and C, right panels). These cell types can be distinguished based on their canonic markers (Fig. 2 B). As expected, SFB colonization increased the frequency of plasma cells and mature T cell subsets (Fig. 2, C–E). In this dataset, four populations of lamina propria CD45⁺ cells expressed *Ifng*, namely conventional CD4⁺ $\alpha\beta$ T cells, CD8⁺ $\alpha\beta$ T cells, NK cells, and NKT cells. Furthermore, NK and CD4⁺ $\alpha\beta$ T cells enhanced *Ifng* expression upon SFB colonization (Fig. 2 F). Using flow cytometry, we confirmed that in WT animals colonized by SFB, the NK cell, NKT cells, as well as further undefined CD3 ϵ [−] population indeed produce IFN γ , but the CD4⁺ and CD8⁺ T cells are by far the most numerous producers of IFN γ in the lamina propria (Fig. 2 G). In summary, both NK and CD4⁺ $\alpha\beta$ T cells increase their *Ifng* production in the presence of SFB, but the latter population is more numerous.

Next, to test whether NK or NKT cells, albeit their low frequency, contribute to the induction of MHCII expression on IECs, we depleted NK and NKT cells using NK1.1 antibody in SFB⁺ WT mice using previously described protocol (Glasner et al., 2018). Although this treatment largely depleted both NK cells (by ~85%) and NKT cells (by ~50%) (Fig. 3 A), we observed no significant effect on the frequency of MHCII⁺ IECs (Fig. 3 B). Thus, we focused on T cells as the major source of IFN γ to determine whether T cells may be the key inducer of the MHCII expression on IECs. We analyzed SFB⁺ Rag1-deficient mice that lack virtually all conventional T cells. To eliminate the possible effect of litter and/or separate housing, we compared Rag1^{−/−}

mice to their Rag1^{+/-} littermates. Using this system, we observed the reduction of MHCII expression on IECs by ~75% in the absence of T cell populations (Fig. 3 C).

To assess directly the effect of T- and NK-derived IFN γ on the MHCII expression on IECs, we utilized IFN γ ^{OFF} mice, in which *Ifng* gene is constitutively inactive (similar to KO), but its activity can be rescued by Cre-mediated recombination (Borst et al., 2020). We crossed this mouse strain to CD4-Cre and Ncr1-Cre mouse strains, leading to rescue of *Ifng* expression potential only in T and NK cell lineages, respectively (Fig. 3 D and Fig. S2 A). Strikingly, IFN γ expression limited to T cells was able to restore MHCII expression on IECs, while NK-restricted IFN γ expression had no measurable effect on epithelial MHCII expression (Fig. 3 E). Collectively, these data prove that IFN γ -producing T cells are both necessary and sufficient to induce MHCII expression on IECs.

Canonically, T cell responses are driven by specific APCs populations. Therefore, we next wanted to determine if SFB-induced IFN γ -producing T cells, responsible for the induction of MHCII on IECs, are also regulated in such a way. Xcr1⁺ cDC1 were recently identified as the major inducers of T_{H1} responses after intestinal infection by epithelial-adhesive cryptosporidium (Russler-Germain et al., 2021). To test whether cDC1 may also be involved in the SFB-mediated induction of MHCII⁺ on IECs, we utilized and analyzed SFB⁺ Xcr1-Cre \times R26-flox-STOP-flox-diphtheria toxin A (Xcr1-DTA) mice (Voehringer et al., 2008; Wohn et al., 2020), in which the mature cDC1 population is depleted by inducible intracellular DTA expression without the disruption of other APC subtypes (Fig. S2, B and C). Strikingly, these mice showed a ~95% decrease in the MHCII expression on their IECs compartment compared with cDC1-sufficient littermates (Fig. 4 A). Furthermore, they almost completely lacked IFN γ expression in both CD4⁺ and CD8⁺ lamina propria T cells, while the frequency of IL-17A-producing CD4⁺ T cells in lamina propria was unaffected (Fig. 4, C and D). Lastly, we inspected if the cDC1 ability to present antigens and activate CD4⁺ T cells is needed for induction of MHCII expression on IECs by selectively depleting MHCII molecule on the cDC1 population (using Xcr1-Cre \times MHCII-fl/fl [MHCII^{cDC1}]) (Fig. S2, B and D). Importantly, MHCII ablation on cDC1 led to a decrease of MHCII expression on IECs by ~75% (Fig. 4 B). This suggests that although both CD4⁺ and CD8⁺ T cells contribute by their IFN γ production to MHCII induction on IECs, CD4⁺ T cells are quantitatively the main source of the IFN γ in this process. Collectively, these results revealed that the regulatory loop responsible for MHCII expression on IECs is based on IFN γ , which is produced mainly by CD4⁺ T cells under the active control of the cDC1 professional APCs population.

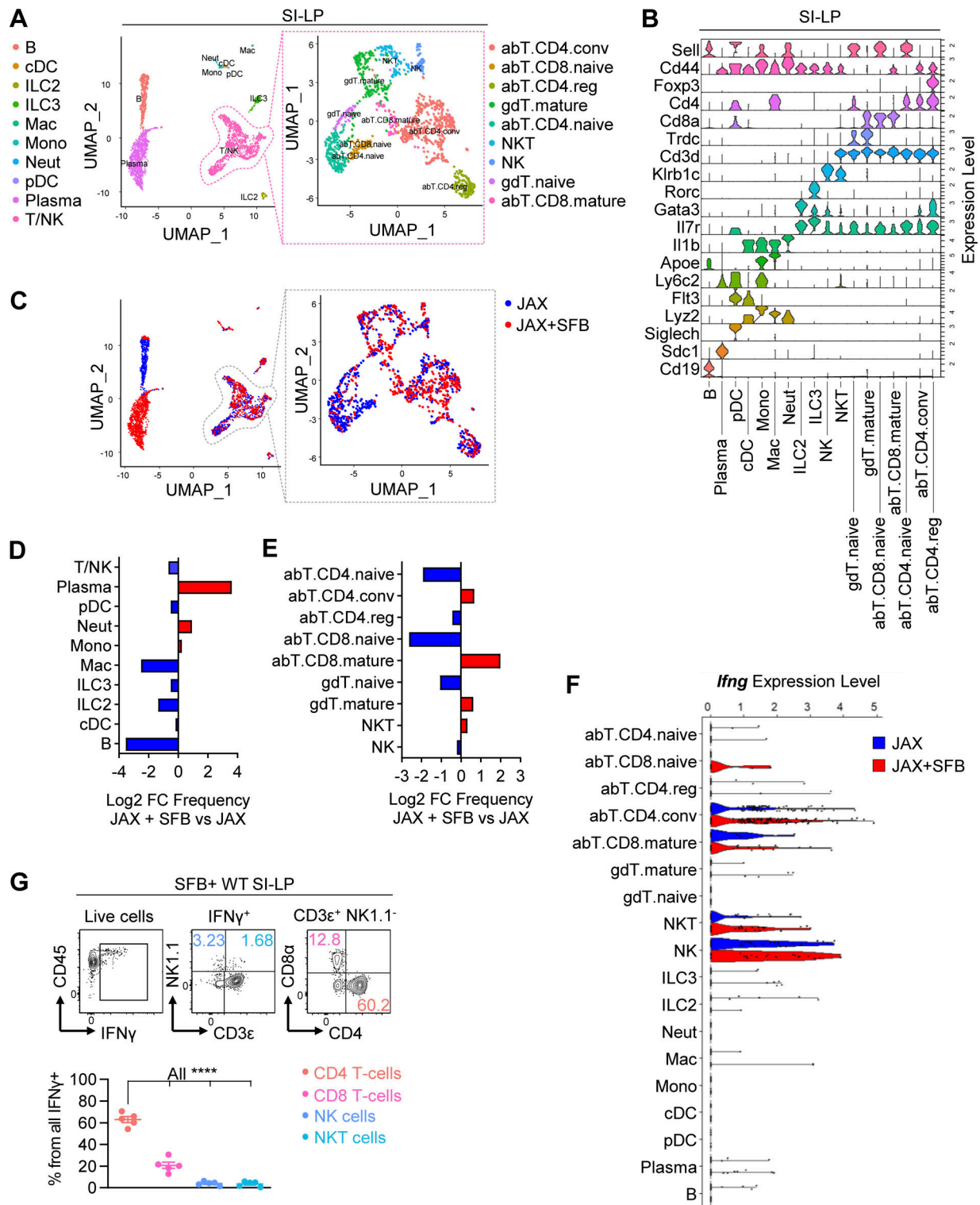


Figure 2. **CD4⁺ T cells are the main producers of IFN γ in SI-LP.** (A–F) scRNA-seq of CD45⁺ SI-LP cells from JAX and JAX + SFB mice. (A) UMAP of annotated cell types. The left plot shows basic clustering, and the right plot shows subclustering of T/NK cluster. (B) UMAP showing the origin of cells from either JAX or JAX + SFB mice. (C) Violin plot of canonic markers defining the identity of clusters to cell types. (D) Graph showing log₂ fold change of frequencies of individual cell types comparing JAX + SFB to JAX mice in basic clustering. (E) Graph showing log₂ fold change of frequencies of individual cell types comparing JAX + SFB to JAX mice in subclustering of T/NK cluster. (F) Violin plot of *Ifng* expression across all the annotated cell types separated by their origin from either JAX or JAX + SFB mice. (G) FACS analysis of the composition of IFN γ -producing cells in SI-LP of SFB colonized mice. Upper plots show representative gating. Bottom plot shows an overview of the data and statistical comparison of CD4 T cells to all other cell types. Numbers beside gates show frequencies from all IFN γ ⁺ cells. Two independent experiments, *n* = 5. Data in G were tested by Student's *t* test. ****, *P* < 0.0001. Horizontal lines show mean \pm SEM.

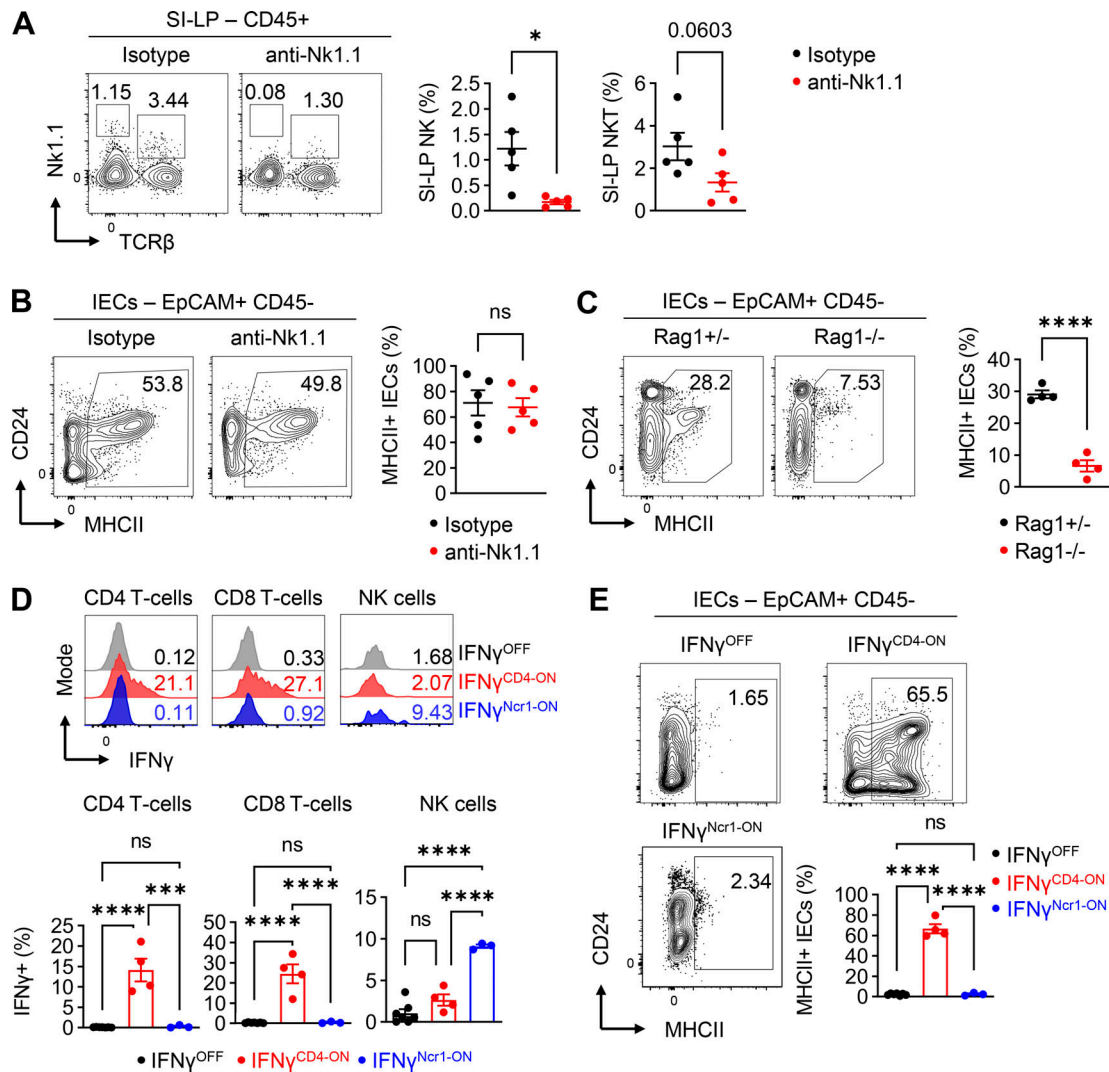


Figure 3. T cell-derived IFN γ drives MHCII expression on the intestinal epithelium. (A and B) SFB-colonized WT mice were injected with 25 μ g of Nk1.1 antibody at 21, 23, 25, 29, 31, and 33 days of age and analyzed at 35 days of age. Two independent experiments, $n = 5$. (A) FACS analysis of NK and NKT cell depletion in SI-LP. Upper plots show representative gating. Bottom plot shows an overview of the data and statistical analysis. Numbers beside gates represent frequency from parent population. (B) FACS analysis of MHCII expression in SI IECs. Plots on the left show representative gating. Plot on the right shows an overview of the results and statistical analysis. Numbers beside gates represent frequency from the parent population. (C) Rag1^{-/-} males were bred with Rag1^{+/-} females, and SI-IECs from their progeny were analyzed by FACS. Plots on the left show representative gating. The plot on the right shows an overview of the results and statistical analysis. Numbers beside gates represent frequency from the parent population. Two independent experiments, $n = 4$. (D and E) Analysis of loxp-STOP-loxp-Irfng (IFN γ ^{OFF}) and their littermates crossed to Cd4-Cre (IFN γ ^{CD4-ON}) or Ncr1-Cre (IFN γ ^{Ncr1-ON}) on SFB⁺ microbiota. (D) FACS analysis of IFN γ production in CD4⁺ T cells, CD8⁺ T cells, and NK cells. Upper plots show representative gating of IFN γ ⁺ cells. Lower plots show overview of the results and statistical analysis. Two independent experiments, $n = 3-7$. (E) FACS analysis of MHCII expression in SI-IECs. Representative gating and statistical overview are shown. Numbers beside gates represent frequencies from parent population. Two independent experiments, $n = 3-7$. Horizontal lines in D and E show mean \pm SEM. Data in A–C were tested by Student’s t test. Data in D and E were tested by ordinary one-way ANOVA with Holm–Šidák’s multiple comparisons test. ns, not significant; *, $P < 0.05$; ***, $P < 0.001$; ****, $P < 0.0001$; in A, P value is shown. Horizontal lines show mean \pm SEM.

MHCII expression on IECs is redundant for T_{H1} and T_{H17} response against SFB

After mechanistically describing steps leading to SFB-induced IFN γ -mediated MHCII expression on IECs, we focused on the physiological role of IEC-expressed MHCII in the context of immune response to SFB. We utilized mice lacking MHCII specifically on their IECs (Villin1-Cre \times MHCII-fl/fl; MHCII^{ΔIEC}) and their Cre-negative littermates (Fig. S2 E). We did not observe any changes in the frequency of IFN γ ⁺ and IL-17A⁺ lamina propria CD4⁺ T cells, pointing to no observable difference in T_{H1} and

T_{H17} responses (Fig. 5 A), in agreement with a previous report (Goto et al., 2014). Thus, we employed an unbiased scRNA-seq analysis of SI IECs from JAX animals and their littermates colonized by SFB to uncover additional changes in the SI IECs expression profile on top of upregulated MHCII expression (Fig. 5 B and Fig. S2 F). We did not observe any expression of costimulatory molecules by IECs, suggesting that the MHCII on IECs might not be involved in the conventional induction phase of the adaptive immune response (Fig. 5 C). However, among the most differentially expressed genes along with MHCII were its

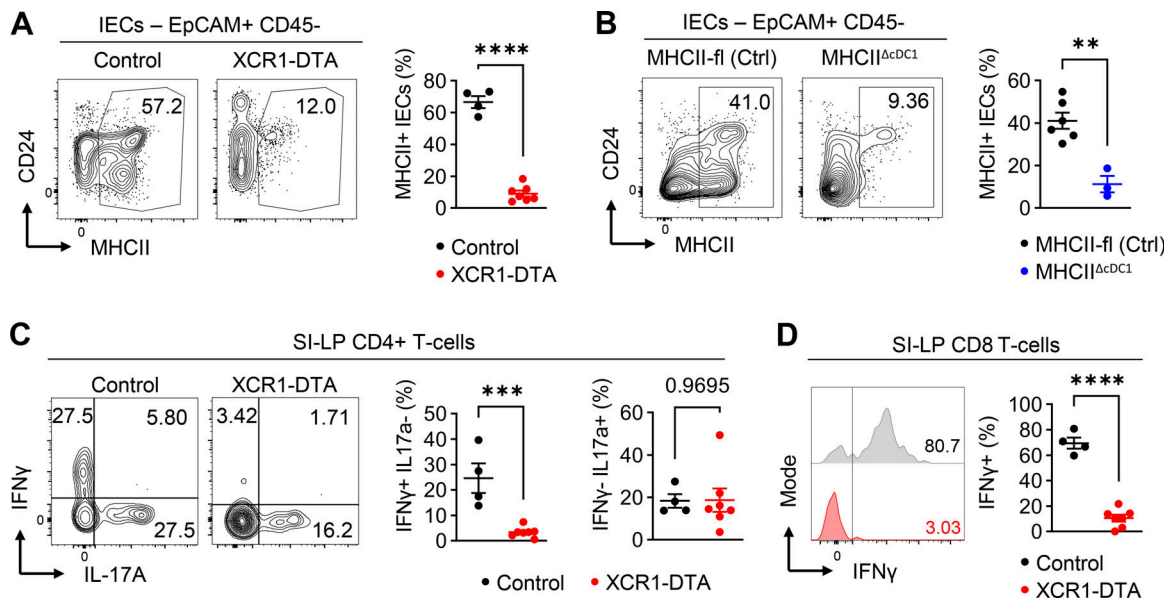


Figure 4. cDC1 control epithelial MHCII expression through regulation of T cell IFN γ production. (A) FACS analysis of MHCII expression in SI-IECs from XCR1-Cre \times Rosa26-loxp-STOP-loxp-DTA (XCR1-DTA) mice and their Cre-negative littermates (control). FACS plots on the left show representative gating. Plot on the right shows an overview of the results and statistical analysis. Three independent experiments, $n = 4-7$. (B) FACS analysis of MHCII expression in SI-IECs from XCR1-Cre \times MHCII-fl (MHCII Δ cDC1) mice and their Cre-negative littermates (MHCII-fl Ctrl). FACS plots on the left show representative gating. Plot on the right shows overview of the results and statistical analysis. Two independent experiments, $n = 3-6$. (C and D) FACS analysis of IFN γ and IL-17a production by CD4 $^+$ T cells (C) or CD8 $^+$ T cells (D) from SI-LP of XCR1-DTA mice and their Cre-negative littermates (control). Plots on the left show representative gating. Plots on the right show overview of the data and statistical analysis. Three independent experiments, $n = 4-7$. All data were tested by Student's t test. **, $P < 0.01$; ***, $P < 0.001$; ****, $P < 0.0001$; P values > 0.05 are shown. Numbers beside gates represent frequencies from parent population. Horizontal lines show mean \pm SEM.

antigen processing machinery members and TLA (*H2-T3*) molecule–ligand for the CD8 α , hallmark marker of the IELs in the gut. All these molecules were predominantly expressed by enterocyte population (Fig. 5 D). In parallel, we also assessed the CD4 $^+$ T cell transcription profile in lamina propria of JAX animals and their littermates colonized by SFB utilizing scRNA-seq. Strikingly, the major expression change we observed in these cells was the massive induction of cytotoxic granzymes in SFB-colonized mice (Fig. 5 E). Since granzymes are highly expressed by IEL (Cheroutre et al., 2011), the upregulation of these molecules in T cells after SFB colonization, together with the elevated expression of *H2-T3* on gut epithelium, suggests the enhanced adaptive IEL-dependent immune response to SFB in the gut of colonized mice.

CD4 $^+$ iIELs accumulate in the intraepithelial space in response to SFB

Our previous experiments suggested that in parallel to canonical T_H17 response, SFB may promote IEL-driven response. To determine the nature and magnitude of this response, we inspected the SI intraepithelial space (SI-IEL) of JAX mice and their SFB-colonized littermates by scRNA-seq (Fig. 5, F and G; and Fig. S3 A). Strikingly, we found that SFB colonization increased the frequency of iIELs among other IEL populations and this increase can be largely attributed to accumulation of CD4 $^+$ iIEL (Fig. 5, G and H). Furthermore, CD4 $^+$ iIEL showed a strong increase in the expression of *Gzmb* after SFB colonization (Fig. 5 I). Since a recent study reported that a subset of IELs can express IL-10 (Tuganbaev et al., 2020), we also checked the expression of

this cytokine in our dataset. IL-10 expression was low regardless of cell type and SFB colonization (Fig. S3 B). Furthermore, this dataset enabled us to confirm that IEL shows low levels of *Ifng* expression in comparison with lamina propria T cells (compare Fig. 2 F and Fig. S3 C).

To validate the ability of SFB to induce IEL response, we analyzed both natural and iIEL populations in JAX mice colonized with SFB and their non-colonized littermates by flow cytometry 2 wk after colonization (Fig. 6 A and Fig. S3 D). The counts of CD4 $^+$ T cells in intraepithelial space increased substantially after SFB colonization (Fig. 6 A). CD4 $^+$ IELs showed increased expression of *Gzmb*, while the CD8a expression remained unaffected (Fig. 6 A). Similar to the previous report (Umesaki et al., 1995), we have also observed the accumulation of CD8 α β iIEL (Fig. S3 D).

To test if the observed effects can be attributed solely to SFB, we monocolonized the GF animals by this microbe (Fig. 6 B and Fig. S3 E). We observed a strikingly similar increase of CD4 $^+$ IELs on frequency and counts accompanied with the enhanced expression of *Gzmb* 2 wk after monocolonization going hand-in-hand with the results observed in JAX animals colonized by SFB on top of their standard microbiota (Fig. 6 B and Fig. S3 E). However, in contrast to SFB colonization of JAX mice, the colonization of GF mice had no effect on the counts of natural IEL (TCR β^+ CD4 $^-$ CD8 β^- and CD3 $^+$ TCR β^-), suggesting that SFB alone specifically induces iIEL response (compare Fig. S3, D and E).

Next, we addressed whether the observed accumulation of *Gzmb* $^+$ CD4 $^+$ iIELs is persistent in the more chronic phase of the

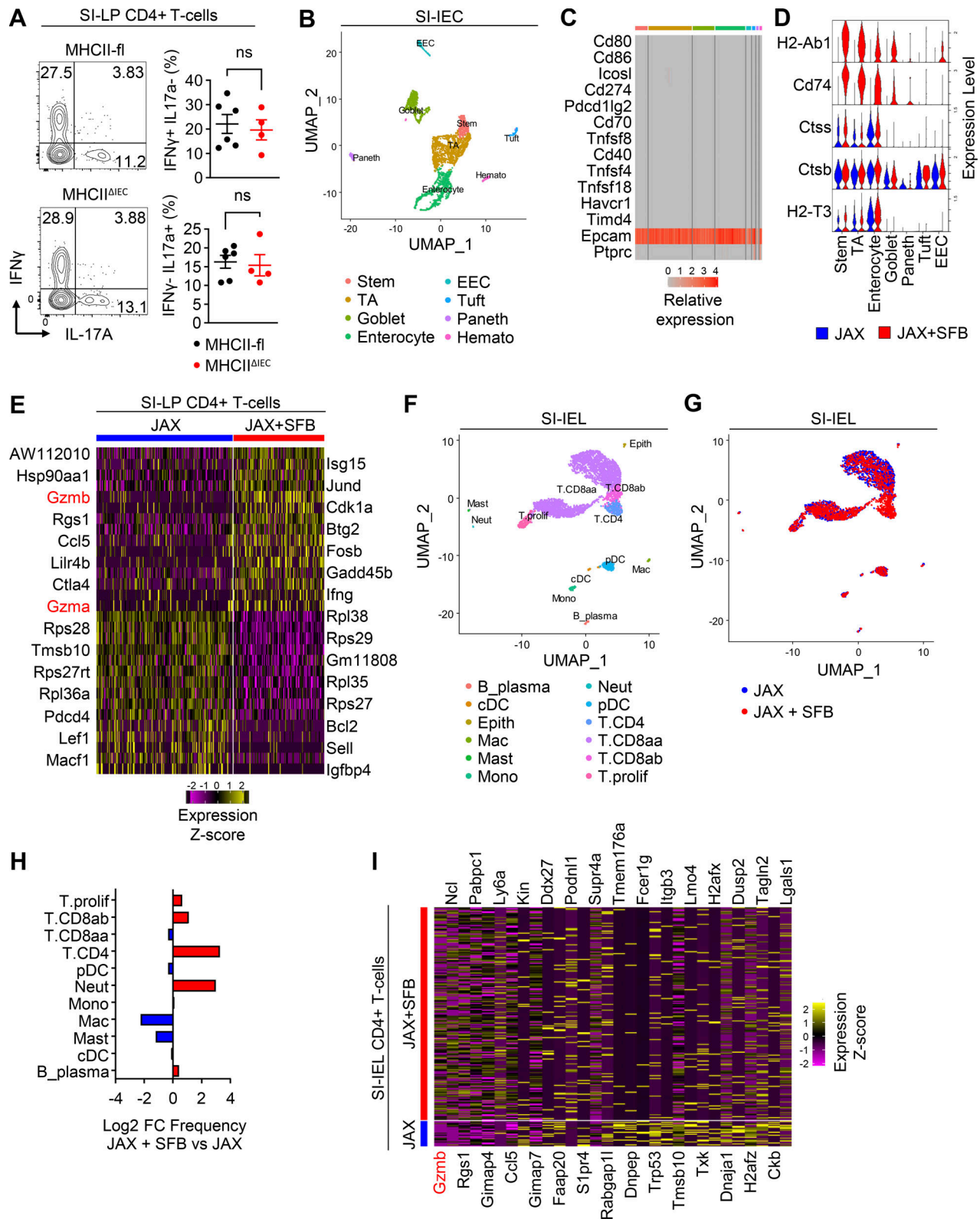


Figure 5. **SFB induce granzyme-expressing CD4 T cells in lamina propria and intraepithelial space.** (A) FACS analysis of IFN γ and IL-17a production by CD4⁺ T cells from SI-LP of *Vil1-CreER* \times *MHCII-fl* mice (*MHCII^{ΔIEC}*) and their Cre-negative littermates (*MHCII-fl*). Plots on the left show representative gating. Plots on the right show quantification of frequencies of IFN γ ⁺ IL-17a⁺ and IFN γ ⁻ IL-17a⁺ in CD3⁺ TCR β ⁺ CD4⁺ T cells. Two independent experiments, $n = 4-7$. (B-D) scRNA-seq of CD45⁻ EPCAM⁺ SI-IECs from JAX and JAX + SFB mice. (B) UMAP of annotated cell types. (C) Heatmap of costimulatory molecules shown as normalized log counts. *Epcam* and *Ptprc* are shown as positive and negative controls, respectively. Cells are separated by their cell type irrespective of the SFB colonization status. (D) Violin plot of MHCII genes (*Cd74*, *H2-Ab1*), genes responsible for MHCII antigen processing (*Ctss*, *Ctsb*), and nonclassical MHC molecule *H2-T3*. Cells are separated by their cell type and SFB colonization status. (E) Heatmap of differentially expressed genes comparing CD4⁺ T cells from SI-LP of

JAX and JAX + SFB mice. Data are shown as z-score of expression. **(F–I)** scRNA-seq of CD45⁺ SI-IEL cells from JAX and JAX + SFB mice. **(F)** UMAP of annotated cell types. **(G)** UMAP showing the origin of cells from either JAX or JAX + SFB mice. **(H)** Plot showing log₂ fold change (FC) of frequency of each cell type comparing JAX + SFB to JAX mice. **(I)** Heatmap of differentially expressed genes comparing CD4⁺ T cells from SI-IEL of JAX and JAX + SFB mice. Data are shown as z-score of expression. Data in A were tested by Student's *t* test. ns, not significant. Numbers beside gates represent frequencies from the parent population. Horizontal lines show mean ± SEM.

colonization or is associated only with the acute phase; thus we measured the intraepithelial space of JAX animals 9 wk after colonization by SFB (Fig. 6 C and Fig. S3 F). We observed a similar increase in the counts of CD4⁺ iIELs; however, in this latter phase, the accumulation of Gzmb⁺ CD4⁺ iIELs was accompanied by their increased expression of CD8 α molecule (Fig. 6 C and Fig. S3 F).

Finally, since SFB were shown to preferentially colonize the distal regions of the SI (Sano et al., 2015), we have also analyzed the distribution of epithelial MHCII expression and CD4⁺ iIELs across the SI. Interestingly, we observed an increase in the MHCII positivity of IECs in the jejunum and ileum sections of the SI (Fig. 7, A–D). This was in parallel mirrored by the increased frequency of Gzmb⁺ CD4⁺ iIELs in these regions (Fig. 7 E).

We have shown that SFB promote the accumulation of various IEL populations, dominated by CD4⁺ iIEL, which primarily upregulate Gzmb and in the later phase after the colonization also CD8 α .

SFB-specific iIELs are dependent on MHCII⁺ IECs

As previous studies showed that MHCII on IEC regulates CD4⁺ iIEL numbers (Bilate et al., 2020; Moon et al., 2021), we sought to determine if this implies also to IELs after the SFB colonization. We utilized SFB⁺ MHCII ^{Δ IEC} mice lacking MHCII expression specifically on intestinal epithelium and their Cre-negative littermates and inspected by FACS analysis of their intraepithelial compartment (Fig. 6 D). Results show that the MHCII expression on IECs regulated the counts of CD4⁺ iIELs while their phenotype as well as other IEL populations remain unaffected (Fig. 6 D and Fig. S3 G).

We next determined whether the observed induction of IELs in bulk population in response to SFB colonization implies also to SFB-specific T cells. To this end, we utilized TCR transgenic mouse strain 7B8, in which all T cells express TCR specifically recognizing SFB-derived antigen bound to MHCII (SFBtg) (Yang et al., 2014). First, we performed a fate-mapping experiment and intravenously transferred CD44-negative naïve CD90.1/2 CD4⁺ SFBtg T cells into WT (CD90.2/2) SFB⁺ recipients (Fig. 8 A). To track these cells, we used the congenic marker CD90.1, allowing a clear distinction between transferred and host T cells (Fig. S4 A).

To inspect all possible fates of SFBtg T cells in the SI, we performed well-based scRNA-seq of lamina propria and intraepithelial α β T cells from mice colonized by SFB harboring adoptively transferred CD90.1⁺ SFBtg T cells. Index flow cytometry-based sorting allowed us to compare protein expression with subsequent transcriptomic analysis and permitted the distinction of SFBtg T cells (TCR β ⁺ V β 14⁺ CD90.1⁺) from host T cells (TCR β ⁺ CD90.1⁻). We were able to define several T cell populations including canonical IELs (Fig. 8 B and Fig. S4 B).

Next, we mapped adoptively transferred SFBtg T cells on the clustering map of the host-derived T cells. Strikingly, the majority of SFBtg T cells fell into the IELs cluster (Fig. 8 C). Furthermore, SFBtg IELs were transcriptionally indistinguishable from canonical IELs (Fig. 8 D) and thus can be designated as bona fide members of the IEL population.

To validate these results, we adoptively transferred SFBtg T cells to SFB colonized WT animals and measured the expression of IEL-associated molecules in mesenteric lymph nodes (mLN), Peyer's patches (PP), SI-LP, and SI-IEL by flow cytometry (Fig. 8 E). Notably, Gzmb and CD8 α expressing SFBtg IELs were present in very low frequencies in mLN, but their numbers gradually increased in PP and lamina propria and were highly enriched in the intraepithelial compartment (Fig. 8, E–G). In summary, these lineage tracing experiments proved that SFBtg CD4⁺ T cells are able to give rise to iIELs.

Having identified another kind of SFB-driven CD4⁺ T cell-based immune response, we asked if this response was impacted by MHCII presence on IECs. To address this question, we constructed bone marrow (BM) chimeric animals, where CD90.2/2 MHCII ^{Δ IEC} served as recipients and 5% of CD90.1/2 SFBtg mice mixed with 95% of WT CD90.2/2 feeder cells served as BM donors (Fig. 8 H). Strikingly, in MHCII ^{Δ IEC} mice, SFBtg T cells were decreased by ~80% in both frequencies and counts in the intraepithelial space compared with their Cre-negative littermates (Fig. 8 I), pointing to the crucial role of MHCII expression on IECs for the proper antigen-specific iIELs response to SFB. In summary, SFB-induced MHCII expression on IECs controls the conversion of SFB-specific CD4⁺ T cell clones to Gzmb⁺ iIELs in the gut intraepithelial space.

IELs navigation by MHCII⁺ IECs is required for control of IEC turnover

The SFB-dependent conversion of CD4⁺ T cells into iIEL suggested that iIELs may in turn control the IEC homeostasis through MHCII-mediated recognition of SFB-infected IECs. To test this hypothesis, we first turned back to our scRNA-seq data of small IECs derived from JAX mice and their littermates colonized by SFB (Fig. 5 B) and used them as the pseudo-bulk of the whole epithelium to compare the cell proliferation and turnover. Indeed, the SFB colonization increased the expression of proliferation markers in SI IECs (*Mki67*, *Top2a*, *Pcna*) (Fig. 9 A). To analyze if these transcriptomic changes indeed reflect changes in IEC turnover rate, we injected JAX mice and their littermates colonized by SFB with 5-ethynyl-2'-deoxyuridine (EdU) that incorporates newly synthesized DNA and analyzed the position of EdU⁺ IECs after 72 h by fluorescent microscopy (Fig. 9, B–D). This time is necessary for IECs to travel from the crypt to the villus tip. Strikingly, the EdU⁺ IECs in JAX mice colonized by SFB were located closer to the villus tip. We inspected the animals

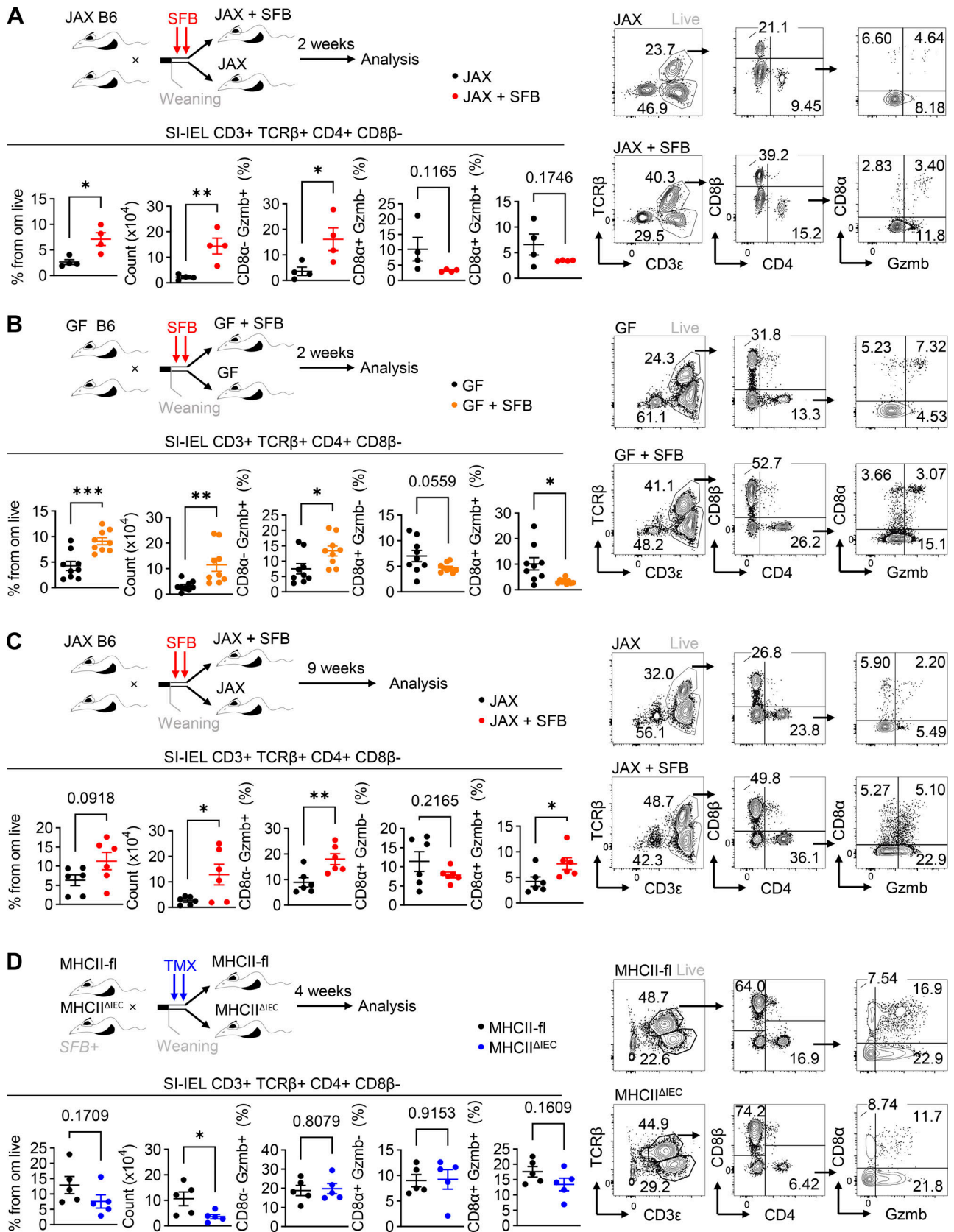


Figure 6. **SFB induce accumulation of Gzmb⁺ CD4⁺ IEL in SI epithelium.** FACS analysis IEL compartment. **(A–C)** JAX (A and C) or GF (B) animals were colonized by SFB at weaning and analyzed after 2 (A and B) or 9 (C) wk. **(D)** MHCII^{ΔIEC} mice and their MHCII-fl littermates were injected by tamoxifen at weaning and analyzed after 4 wks. **(A–D)** Schematic on the top of each panel shows the experimental setup. FACS plots on the right show representative

gating. Plots on the bottom of each panel show quantification of frequencies and counts of CD3⁺ TCRβ⁺ CD4⁺ CD8β⁻ CD4 T cells and the frequencies of CD8α⁻ Gzmb⁺, CD8α⁺ Gzmb⁻, and CD8α⁺ Gzmb⁺ cells from CD4⁺ T cells. Two independent experiments, *n* = 4 (A); three independent experiments, *n* = 9 (B); two independent experiments, *n* = 6 (C); two independent experiments, *n* = 5 (D). All data were tested by Student's *t* test. *, *P* < 0.05; **, *P* < 0.01; ***, *P* < 0.001; *P* values >0.05 are shown. Numbers beside gates represent frequencies from the parent population. Horizontal lines show mean ± SEM.

2 wk (Fig. 9 B) and 9 wk after SFB colonization (Fig. 9 C), validating that SFB presence promotes turnover and proliferation of the intestinal epithelium in acute as well as in the more chronic timepoint.

Next, we inspected if the regulation of IECs turnover is dependent on IEC-expressed MHCII and thus potentially on SFB-induced CD4⁺ iIEL, as the MHCII ablation leads to the striking decrease of SFB-specific IELs (Fig. 8 I). To analyze this, we performed the EdU assay in the same setting as before, using MHCII^{ΔIEC} mice and their Cre-negative littermates (Fig. 9 D). In contrast to SFB colonization, MHCII ablation on IECs decreased the proximity of EdU⁺ IECs to the villus tip (Fig. 9 D), suggesting that MHCII on IECs and in turn SFB-specific CD4⁺ IELs are instrumental for regulation of IECs turnover. However, it should be noted that the magnitude of the decrease is milder than the effect of SFB colonization (Fig. 9, B and C).

To inspect this more in detail, we established FACS protocol allowing us to measure the frequency of mature enterocytes in the SI epithelium (Fig. S5) and utilized it to determine changes in epithelial compartment composition in JAX mice and their littermates colonized by SFB. We observed the increased frequency of mature enterocytes after SFB colonization (Fig. 9 E), while the MHCII ablation on IECs using the MHCII^{ΔIEC} mice led

to a decrease in enterocyte frequency (Fig. 9 F), albeit this effect was weaker than the effect of SFB colonization. Finally, to inspect the direct role of SFB-specific CD4⁺ iIELs in the regulation of turnover of mature enterocytes, we used a SI organoid culture. The addition of the SFB-specific iIELs into the culture led to the increased frequency of mature enterocytes in the culture (Fig. 9 G), providing a direct link between iIELs presence and the changes in epithelial cells compartment.

Collectively, our data show that SFB promote the MHCII expression on IECs via the induction of IFNγ production in SI T cells in a cDC1-dependent manner. In turn, MHCII⁺ IECs control the conversion of granzyme⁺ CD4⁺ CD8α⁺ iIELs originating from SFB-specific conventional CD4⁺ T cells. These iIELs in turn regulate the IECs turnover and mature enterocytes pool in MHCII-navigated and dependent manner.

Discussion

Our study describes a previously uncharacterized type of immune response against SFB, a commensal bacterium of *Clostridia* taxon living in close association with IECs. This immune response starts with SFB-driven induction of IFNγ expression in intestinal T_H1 cells in a cDC1-dependent manner. Subsequently,

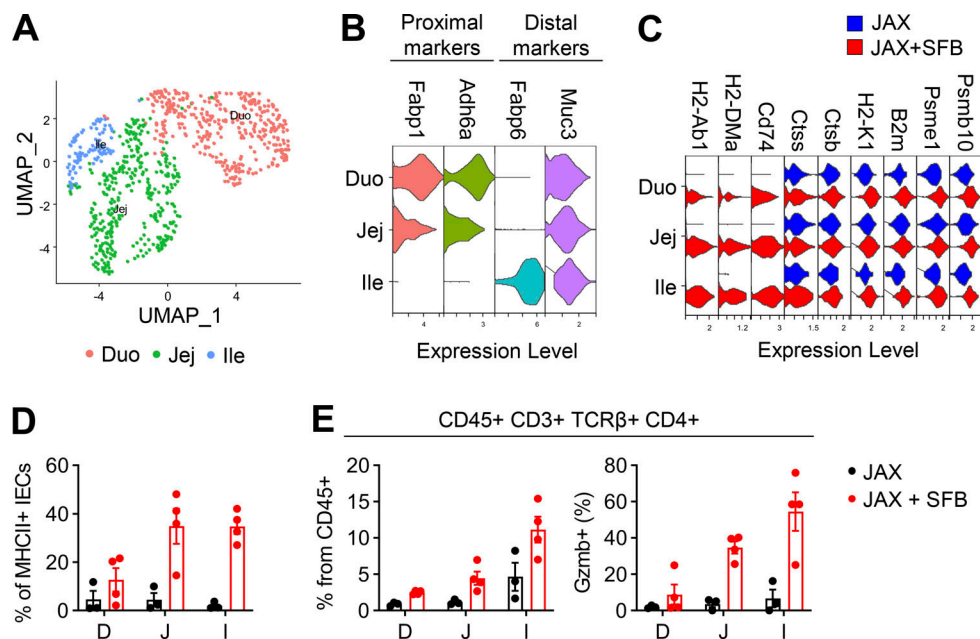


Figure 7. **MHCII on IECs and CD4⁺ iIEL accumulate in distal regions of the SI.** (A–C) scRNA-seq analysis of enterocytes from dataset shown in Fig. 4. Enterocytes were subclustered, and their origin from duodenum (Duo), jejunum (Jej), and ileum (Ile) (A) was identified based on previously published markers (B) (Haber et al., 2017). (C) Violin plot of MHC I and MHC II expression and other molecules involved in antigen presentation. (D and E) FACS analysis of epithelial MHCII (D) and CD4⁺ IELs (E) from 5-wk-old JAX mice, half of which was colonized with SFB at weaning. Data in D shows the frequency of MHCII⁺ cells from IECs in each intestinal segment. (E) Left plot shows the frequency of CD4⁺ IELs. Right plot shows the frequency of Gzmb⁺ cells from CD4⁺ IELs. Three independent experiments, *n* = 3–4 (D and E). Horizontal lines show mean ± SEM.

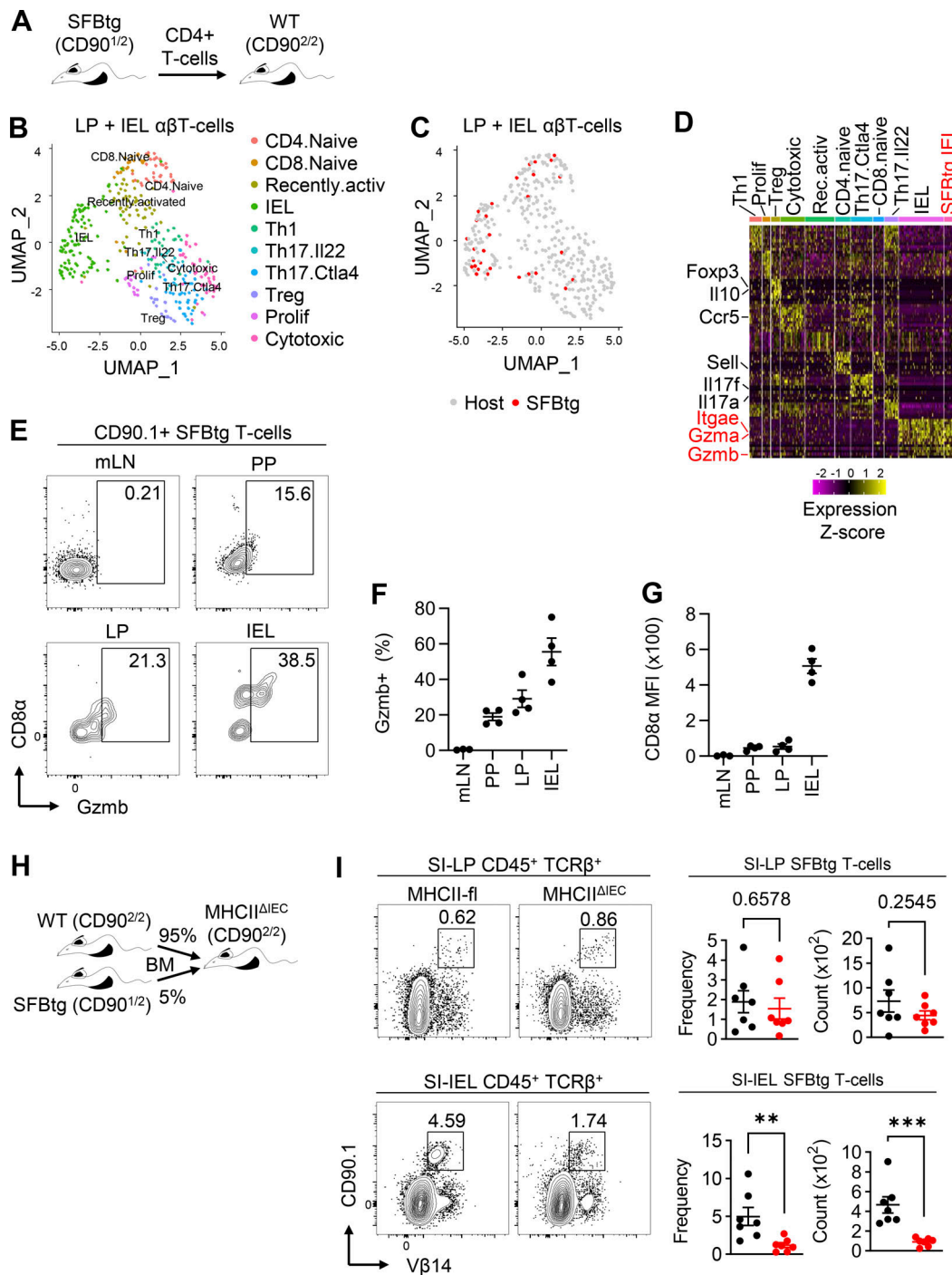


Figure 8. SFB induce a switch of cognate CD4 T cells to granzyme-expressing IEL dependent on epithelial MHCII. (A–G) CD90.1/2 CD4 T cells carrying transgenically expressed TCR, specific for SFB antigen (SFBtg) were adoptively transferred to CD90.2/2 mice. (A) Schematic of the experimental setup. (B–D) scRNA-seq of TCR β^+ SI-LP and SI-IEL cells. (B) UMAP of annotated cell types. (C) UMAP showing the origin of cells from either donor (SFBtg) or host mice (polyclonal). (D) Heatmap of differentially expressed genes that define cell types among host cells, shown in all host cell types and SFBtg T cells from IEL cluster. Data are shown as z-score of expression. (E–G) FACS analysis of SFBtg T cell mLN, PP, SI-LP, and SI-IEL. (E) Representative FACS plots of CD8 α and Gzmb and gating for Gzmb $^+$ cells. (F) Plot showing the frequency of Gzmb $^+$ cells among SFBtg T cells in mLN, PP, SI-LP, and SI-IEL. Two independent experiments, $n = 3-4$. (G) Plot showing the MFI of CD8 α cells in SFBtg T cells in mLN, PP, SI-LP, and SI-IEL. Three independent experiments, $n = 3-4$. (H and I) BM from SFBtg (CD90.1/2) and WT (CD90.2/2) mice were mixed in 5:95 ratio and i.v. injected into lethally irradiated MHCII Δ IEC mice and their Cre-negative littermates (MHCII-fl), which were both i.p. injected with 1 mg of tamoxifen in 50 μ l of sunflower oil at 21 and 22 days of age. Mice were analyzed 6 wk after BM transplantation. (H) Schematics of the experimental setup. (I) FACS analysis of counts and frequencies of SFBtg T cells in SI-LP and SI-IEL. Plots on the left show representative gating. Plots on the right show overview of the results and statistical analysis. Three independent experiments, $n = 7$. Data in I were tested by Student's t test. **, $P < 0.001$; ***, $P < 0.0001$; P values >0.05 are shown. Numbers beside gates represent frequencies from parent population. Horizontal lines show mean \pm SEM.

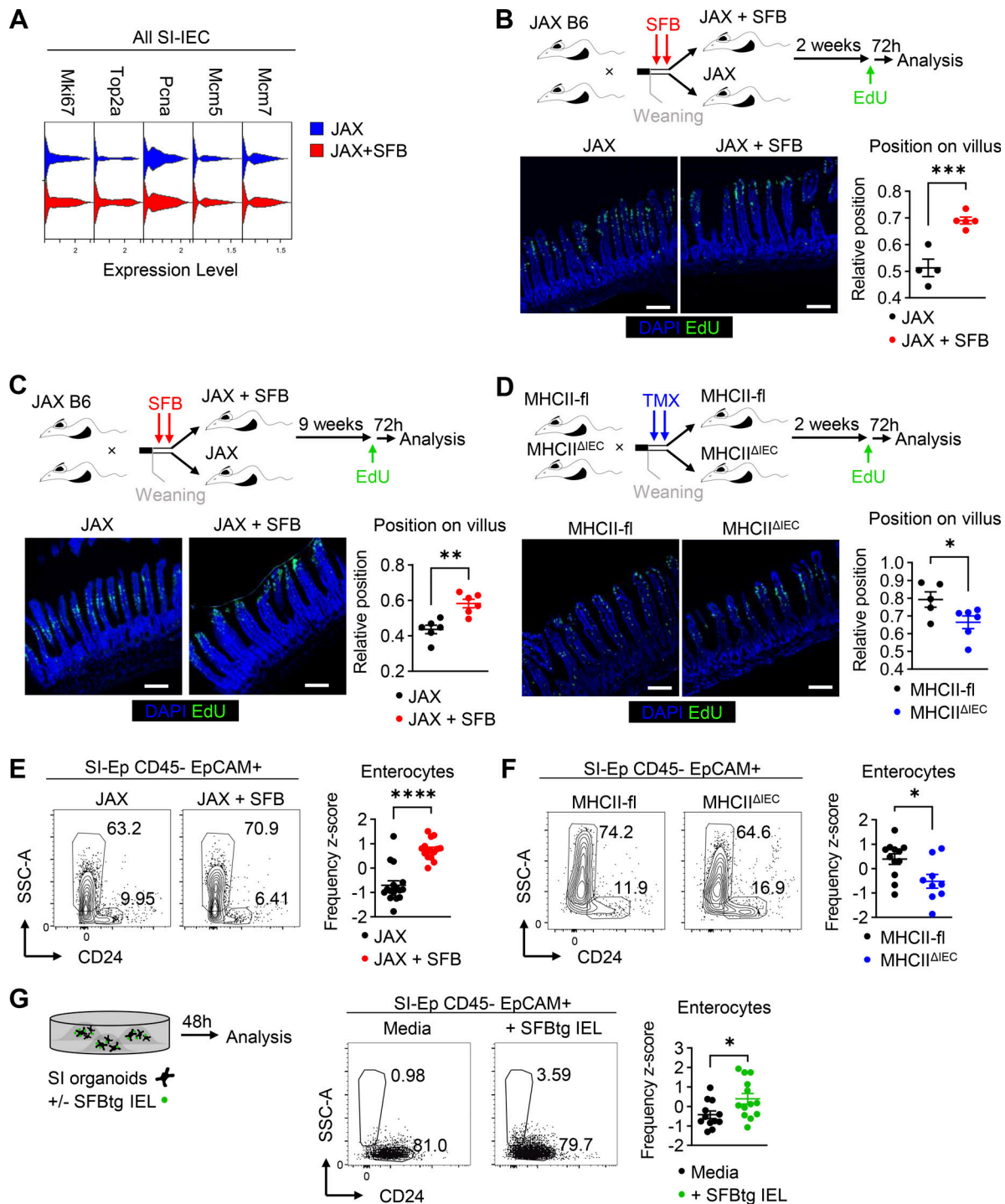


Figure 9. **SFB colonization, epithelial MHCII, and SFB-specific IEL control epithelial turnover.** (A) Expression of proliferation signature genes in IECs from JAX and JAX + SFB mice, analyzed by scRNA-seq, shown across all IECs irrespective of their cell type. (B) Analysis of the epithelial turnover rate using EdU in JAX mice colonized with SFB at weaning and their non-colonized littermates, both analyzed at 5 wk of age. (C) Analysis of the epithelial turnover rate using EdU in JAX mice colonized with SFB at weaning and their non-colonized littermates, both analyzed at 12 wk of age. (D) Analysis of the epithelial turnover rate using EdU in MHCII^{ΔIEC} mice and their Cre-negative littermates (MHCII-fl), both analyzed at 5 wk of age. (B–D) Mice were i.p. injected with 1.25 mg of EdU 72 h prior to the analysis. Schematic on the top of each panel shows the experimental setup. Representative microscopic images and quantification of the relative position of EdU⁺ cells on the villus are shown below. Scale bar represents 100 μ m. Two independent experiments, $n = 4–5$ (B); two independent experiments, $n = 6$ (C); two independent experiments, $n = 5–6$ (D). (E) FACS analysis of enterocyte frequency in JAX mice colonized with SFB at weaning and their non-colonized littermates, both analyzed at 5 wk of age. Five independent experiments, $n = 15–16$. (F) FACS analysis of enterocyte frequency in MHCII^{ΔIEC} mice and their Cre-negative littermates (MHCII-fl), both analyzed at 5 wk of age. Four independent experiments, $n = 9–12$. (E and F) FACS plots on the left show representative gating. Plots on the right side of each panel show quantification of enterocyte frequency. Values are shown as z-score calculated individually for each experiment to eliminate batch effect. (G) Analysis of the effect of SFB-specific IEL on the differentiation of enterocytes in SI organoids. Organoids were

generated from SI crypts and maintained in culture for 4 days. On day 5 of the culture, IFN γ (10 ng/ml) and SFB-derived cognate peptide (1 ng/ml) were added to the culture media. On day 6 of the culture, freshly isolated IEL from SFB-colonized SFBtg mice were added to the culture in 1:5 ratio (IEL:organoid cells). To ensure proper binding of IEL to organoids, organoids were harvested and incubated with IEL for 1 h at 37°C. This combined culture was carried out for 48 h in the presence of IFN γ and SFB-derived cognate peptide. Afterward, organoids were harvested, and the frequency of enterocytes was analyzed by FACS. The schematic on the left shows experimental setup. FACS plots show representative gating. The plot on the right side of each panel shows quantification of enterocyte frequency. Values are shown as z-score calculated individually for each experiment to eliminate batch effect. Four independent experiments, $n = 12$ – 13 . All data were tested by Student's t test. *, $P < 0.05$; **, $P < 0.01$; ***, $P < 0.001$; ****, $P < 0.0001$.

the T_{H1}-derived IFN γ induces massive expression of MHCII on IECs. In parallel, SFB colonization induces differentiation of SFB-specific CD4⁺ T cell clones into granzyme-expressing iIELs in the latter phase bearing the CD8 α , which accumulate in the intestine but are severely diminished in numbers when MHCII on IECs is ablated. Finally, we show that SFB-specific iIEL response ultimately regulates the turnover of IECs in MHCII-dependent manner.

While previous studies described the importance of T_{H17} response against SFB (Gaboriau-Routhiau et al., 2009; Ivanov et al., 2008, 2009), this study shows that in addition to this well-established mechanism, the immune reaction targeted against SFB also involves T_{H1} and cytotoxic iIELs responses. Spatially, the T_{H1} and T_{H17} responses against SFB are preferentially localized in the lamina propria, where IFN γ induces MHCII expression on IECs and T_{H17} effector cytokines induce recruitment of neutrophils (Flannigan et al., 2017), promote antimicrobial peptide production (Shih et al., 2014), and enhance epithelial healing (Pickert et al., 2009). In contrast, the iIEL response is localized in the intraepithelial space and propagates the renewal of the SFB-stressed gut epithelium by increasing its turnover rate.

Although previous studies described that SFB are able to induce MHCII expression in IECs (Goto et al., 2014; Tuganbaev et al., 2020; Umesaki et al., 1995), the immune signals used by SFB-driven response to induce MHCII on IECs were poorly defined. We build on previous knowledge that MHCII expression in the intestinal epithelium is dependent on IFN γ (Al Nabhani et al., 2019; Koyama et al., 2019; Thelemann et al., 2014; Van Der Kraak et al., 2021) and show that SFB-driven induction of IFN γ cytokine in intestinal lamina propria T cells is indispensable for their ability to drive MHCII on IECs. Our results stress that while the expression of MHCII in the intestinal epithelium is IFN γ -induced, IFN γ produced during weaning is not sufficient for the long-lasting MHCII expression on IECs. Our study suggests that the SFB-induced T_{H1} response is kept in equilibrium with the T_{H17} response through a feedback loop since IFN γ is the main inducer of MHCII expression in IECs, while IL-17A acts in an opposite manner. Interestingly, it was recently shown that similar to the effect of SFB-attachment on Th17 response, SFB-induced MHCII on IECs is largely dependent on the ability of SFB to attach to IECs as well (Tuganbaev et al., 2020). However, in contrast to T_{H17} response, SFB-induced MHCII on IECs shows only partial dependence on the expression of serum amyloid proteins (Tuganbaev et al., 2020), and it is completely independent of Cdc42, small GTPase responsible for SFB endocytosis (Ladinsky et al., 2019; Tuganbaev et al., 2020). On the other hand, we show that SFB-induced IFN γ production by T_{H1} cells and in turn their ability to induce MHCII on IECs is completely

dependent on the antigen presentation by cDC1 population. Together, these results suggest that T_{H1}/IEL and T_{H17} branches of SFB-induced immune responses are regulated by largely distinct mechanisms.

However, the only common factor necessary for SFB to induce both T_{H1} and T_{H17} responses—their attachment to IECs—might be also the defining factor for the induction of T_{H1}-mediated IEC-MHCII-dependent induction of iIEL responses in general. First, the recently discovered strain of epithelium-tightly associated *Cryptosporidium* was shown to drive T_{H1} responses in a cDC1-dependent manner. Furthermore, while this microbe is well tolerated in WT mice, mice with disrupted cDC1 compartments succumbed to death after colonization (Russler-Germain et al., 2021). Second, it was reported that colon-residing *Citrobacter rodentium* and *Helicobacter hepaticus*, both epithelial-attaching intestinal pathogens, are able to induce MHCII expression on colonic IECs (Heuberger et al., 2023). *C. rodentium* as well belongs to the group of attaching and effacing bacteria and often serves as the animal model for human enterotoxigenic *Escherichia coli* infections (Collins et al., 2014; Wiles et al., 2006). This further highlights the importance of MHCII expression on the IECs in the regulation of immune response against microbes living tightly associated with IECs.

One of the previously unresolved questions is how mechanistically MHCII on IECs can regulate response to bacteria that induce it, particularly since epithelial expression of MHCII is redundant for the induction of T_{H17} response (Goto et al., 2014), which was classically studied in this context. We have shown that the major function of MHCII on IECs is the regulation of the cellularity of IELs that recognize bacteria inducing MHCII on IECs. Importantly, we were able to show by lineage tracing experiments that these iIELs are generated from SFB-specific CD4⁺ conventional T cells. Moreover, SFB-specific iIELs are transcriptionally undistinguishable from bona fide IELs. Interestingly, recent studies showed that IECs regulate CD4⁺ CD8 α ⁺ iIEL development through MHCII-mediated antigen presentation (Bilate et al., 2020; Moon et al., 2021) and that TCR derived from peripherally generated Tregs (pTreg) reactive to commensal microbiota antigens predestines T cells to differentiate to CD4⁺ iIEL (Bilate et al., 2016). However, once the cognate peptide, derived from β -hexosaminidase, an enzyme conserved throughout the Bacteroidetes phylum, was identified, it became clear that microbes which provide the antigenic target for pTreg-TCR-derived CD4⁺ iIEL are unable to drive the generation of these iIEL alone since they are unable to induce the expression of MHCII on IECs (Bousbaine et al., 2022). Here, we show that in contrast to Bacteroidetes, which were the first identified antigenic target of iIELs in a complex study by Bousbaine et al. (2022), SFB are able to drive both MHCII

expression in IECs and the accumulation of CD4⁺ iIEL, which are generated from conventional SFB-specific CD4⁺ T cells. Thus, it seems that SFB-specific and Bacteroidetes-specific iIEL might be generated by slightly different mechanisms, but both share the dependence on the epithelial MHCII expression.

It should also be clarified that in the aforementioned study, authors claim that SFB colonization does not induce the generation of CD4⁺ iIEL (Bousbaine et al., 2022), and similarly, the monoassociation of GF animals with SFB was previously shown to have minimal effect on CD4⁺ iIEL (Mucida et al., 2013). However, this interpretation is based on the finding that CD4⁺ T cells do not upregulate CD8 α expression in the intraepithelial space after SFB colonization of JAX mice or GF animals (Bousbaine et al., 2022; Mucida et al., 2013). Using the comparable setup, we show that SFB colonization leads to the accumulation of CD4⁺ iIELs, despite the lack of CD8 α expression, both relative to other IELs populations as well as in total counts of CD4⁺ iIELs. Our data also confirm that SFB colonization does not induce CD8 α expression on CD4⁺ granzyme-positive iIELs during the acute phase of the immune response. However, the increased CD8 α can be readily detectable in the more chronic phase of the immune response against SFB in the bulk population as well as on SFB-specific iIELs. Interestingly, a similar phenomenon, the accumulation of CD4⁺ T cells in the intraepithelial space without the induction of CD8 α expression was reported in a recent study focusing on food antigen-specific iIELs (Lockhart et al., 2023). Similar to SFB, the *Lactobacillus reuteri* is able to drive the generation of CD4⁺ iIEL even in the absence of other microbes (Cervantes-Barragan et al., 2017). However, since neither the ability of *L. reuteri* to induce epithelial MHCII nor the antigenic specificity of *L. reuteri*-induced CD4⁺ iIEL has been assessed so far, it is unclear if *L. reuteri* uses a similar mechanism as SFB to drive CD4⁺ iIEL response or if *L. reuteri*-induced CD4⁺ iIEL bypass the requirement for the epithelial MHCII expression. Thus, the antigen-specific CD4⁺ iIEL response coupled with MHCII expression on IECs, which are both induced by SFB, identifies this commensal as the only microbe able to drive the full-fledged CD4⁺ iIEL, described so far.

In the broader scope of MHCII's role on IECs, there have been some seemingly conflicting reports regarding the role of MHCII in the maintenance of intestinal homeostasis in mice. Specifically, while MHCII expression on IECs protects the host from infectious colitis (Jamwal et al., 2020), it was found to aggravate chemical and T cell-induced colitis (Jamwal et al., 2020; Tuganbaev et al., 2020). Similarly, while MHCII on IECs was found to protect the host from the development of intestinal cancer (Beyaz et al., 2021), its expression on IECs was suggested to serve as the target for allogenic T cells and thus drive graft-versus-host disease (Koyama et al., 2019). We believe that the mechanistic insight we show in this study can clarify this issue. We have shown that useful members of CD4⁺ T cell repertoire with proven specificity for IEC-attaching bacteria are able to express molecules necessary for tight association with the IECs and granzymes. Thus, they are acquiring cytotoxic potential together with the ability to migrate to intraepithelial space. Strikingly, this process is dependent on the epithelial expression of MHCII molecules.

It is thus possible to hypothesize that the immune system evolved a specific strategy, that is responsible for controlling bacterial strains tightly associated with IECs. The control is based on MHCII navigation of the cytotoxic, bacterium-specific iIEL response which is able to increase the IECs turnover. Strikingly, this scenario can easily explain some previously reported observations since such a mechanism would be beneficial if the immune system fights invading pathogens (Jamwal et al., 2020) or keeps in check commensals to prevent their overgrowth (Russler-Germain et al., 2021). On the other hand, it could cause severe damage, when the immune system targets gut epithelial cells without discrimination (in a state of graft-versus-host disease) (Koyama et al., 2019), or if the cytotoxic response to commensals gets out of control (like in inflammatory bowel disease) (Jamwal et al., 2020; Tuganbaev et al., 2020). It can also explain why the absence of MHCII on IECs can predispose epithelium to malignant transformation (Beyaz et al., 2021) since the abrogation of immune surveillance by IELs and the disruption of possible cytotoxic elimination of (pre)malignant cells can be precisely the causative factor.

The mechanism we describe here may also have important implications for the regulation of antiviral intestinal responses. While a recent study showed that SFB protects the host from rotavirus infection by increasing epithelial turnover and shedding of infected cells (Shi et al., 2019), another report recently showed that iIEL derived from CD4⁺ T cells protected the host from the infection with intestinal viral infections in IFN γ -dependent manner (Parsa et al., 2022). Our data suggest that the protective effect of SFB can act through the IFN γ -dependent induction of MHCII on IECs and concomitant switch of conventional SFB-specific CD4⁺ T cells to iIEL with cytotoxic potential that can convey the protection from the virus through the increase in the epithelial turnover. Thus, the immune response described herein, and its defective regulation may have devastating (patho)physiologic consequences ranging from impaired clearance of invasive epithelia-associated bacteria to chronic intestinal inflammation or intestinal cancer.

Materials and methods

Mice

All mice used in this study were on C57Bl/6J background. Mice were used irrespective of their sex since we did not observe any sex-dependent differences in the analysis we performed. C57Bl/6J animals were shipped directly from the Jackson Laboratory (JAX: 000664). SFB-negative status of these animals was confirmed by quantitative PCR (qPCR) and Gram-staining from their faces. To keep the microbiota of these animals identical to that present in JAX, mice were directly transferred to the Trexler-type plastic isolator in the Laboratory of Gnotobiology straight after shipping and maintained isolated further on. These mice were provided with autoclaved tap water and rodent diet (V1126-000; Ssniff) and bedding was sterilized by irradiation 50 kGy (Bioster). Locally derived GF mice were maintained in the same manner as mice shipped from JAX. All other mouse strains were housed under standard specific pathogen-free conditions in individually ventilated cages. R26-fl-STOP-fl-DTA

(B6.129P2-Gt(ROSA)26Sortm1(DTA)Lky/J, 009669) (Voehringer et al., 2008), H2-Ab1^{fl/fl} (MHCII-fl, B6.129×1-H2-Ab1tm1Koni/J, 013181) (Hashimoto et al., 2002), Rag1^{-/-} (B6.129S7-Rag1tm1-Mom/J, 002216) (Mombaerts et al., 1992), CD90.1 (B6.PL-Thy1a/CyJ, 000406), CD4-Cre (B6.Cg-Tg(Cd4-cre)1Cwi/BfluJ, 22071) (Lee et al., 2001), and SFBtg (Tg(Tcra,Tcrb)2Litt/J, 027230) (Yang et al., 2014) mouse strains were purchased from JAX. IFN γ ^{OFF} (B6.129P2-Ifngtm1Uka) (Borst et al., 2020) mice were kindly provided by Dr. Ulrich Kalinke (TWINCORE, Hanover, Germany). Ncr1-Cre mice (Eckelhart et al., 2011) were kindly provided by Dr. Veronika Sexl (Medical University of Vienna, Vienna, Austria). Xcr1-Cre (Xcr1-IRES-iCre-GSG-2A-mTFP) (Wohn et al., 2020) animals were kindly provided by Dr. Bernard Malissen (Centre National de la Recherche Scientifique, Marseille, France). Vill1-CreERT (B6.Cg-Tg(Vill1-cre/ERT2)23Syr/J) (el Marjou et al., 2004) mice were kindly provided by Dr. Vladimir Korinek (Czech Academy of Sciences, Prague, Czech Republic). All mice were given a standard rodent high-energy breeding diet and reverse osmosis-filtered water ad libitum. Mice were kept at a 12 h/12 h light/dark cycle; temperature and relative humidity were maintained at 22 ± 1°C and 55 ± 5%, respectively. All experiments were approved by the ethical committee of the Faculty of Science of Charles University, the ethical committee of the Institute of Molecular Genetics of the Czech Academy of Science, and the ethical committee of the Institute of Microbiology of the Czech Academy of Science.

Cell isolations

For the isolation of SI epithelium, SI-LP, and SI-IEL cells, we euthanized the mouse by cervical dislocation, dissected complete SI, and maintained it in PBS on ice. SI was then cleaned from mesenteric fat and luminal contents were rinsed with ice-cold PBS using a syringe. Equal portions (6 cm) of each of the SI segments—duodenum, jejunum, and ileum—were then cut, and the rest of the tissue was discarded. PP were excised carefully, and the remaining tissue was cut open longitudinally and separated into 2-cm long pieces. This tissue served as the input material for the downstream isolation methods.

For the isolation of SI epithelium, tissue was incubated in HBSS without Ca²⁺ and Mg²⁺ supplemented with 3% fetal bovine serum (FBS; Gibco) and 2 mM EDTA (stripping buffer) on ice for 90 min, followed by 10 s of vortexing. Tissue was transferred to a fresh stripping buffer and incubation/vortexing was repeated several times, with 30-min incubation time, and the stripping buffer containing pieces of the epithelium was collected. For the analysis of complete SI epithelium (crypts and villi), second and third fractions were pooled and used further. For the analysis of crypt-resident epithelial cells, the fourth and fifth fractions were passed through a 100- μ m nylon filter and pooled together. For the isolation of villi, the first fraction was passed through a 100- μ m nylon filter, and the flowthrough was discarded. Villi were eluted from the filter in the stripping buffer. Epithelium was then collected by centrifugation (3 min, 300 g, 4°C) and digested by TrypLE express (Gibco) for 1 min at 37°C and vortexed. The cell suspension was passed through a 100- μ m filter, washed with stripping buffer, and used for downstream applications.

For the isolation of SI-IEL cells, SI tissue was incubated in the stripping buffer at 37°C for 20 min. This procedure was repeated one more time and the buffer containing the epithelium was pooled, collected by centrifugation, and digested by TrypLE express for 1 min at 37°C and vortexed. The cell suspension was passed through a 100- μ m filter and washed with a stripping buffer. IELs were enriched by Percoll (Cytiva) gradient centrifugation. Specifically, cells were resuspended in 4 ml of 40% Percoll in RPMI medium (Gibco) supplemented with 3% FBS. This suspension was then underlaid with 2 ml of 80% Percoll in RPMI medium supplemented with 3% FBS. This gradient was centrifuged for 20 min at 800 g at 21°C without brake. IEL cells were collected from the interface, washed with stripping buffer, and used for downstream applications.

For the isolation of SI-LP cells, SI tissue was stripped of the epithelium in the same way as for the isolation of SI-IEL. The remaining tissue was then cut to ~2 mm pieces and incubated in an enzymatic cocktail at 37°C for 1 h. This cocktail contained Collagenase D (1 mg/ml; Roche) and DNase I (40 U/ml; Roche) dissolved in RPMI medium supplemented with 3% FBS. The tissue was then vortexed for 10 s and passed through a 100- μ m filter. The remaining tissue was meshed on a 100- μ m cell strainer. Cells collected by mashing were pooled with the flow-through, washed with the stripping buffer, and collected by centrifugation. LP cells were isolated by Percoll gradient centrifugation. Cells were resuspended in 4 ml of 40% Percoll in RPMI medium supplemented with 3% FBS. This suspension was then underlaid with 2 ml of 80% Percoll in RPMI medium supplemented with 3% FBS. This gradient was centrifuged for 20 min at 800 g at 21°C, without brake. Cells were collected from the interface, washed with stripping buffer, and used for downstream applications.

For the isolation of T cells for the adoptive transfer spleen, axillary, brachial, inguinal, and cervical lymph nodes were dissected. These tissues were cut into ~2 mm pieces and incubated for 1 h at 37°C in the enzymatic cocktail containing Collagenase D (1 mg/ml; Roche) and DNase I (40 U/ml; Roche) dissolved in RPMI medium supplemented with 3% FBS. The tissue was then vortexed for 10 s and passed through a 100- μ m filter. The remaining tissue was meshed on a 100- μ m cell strainer. Cells collected by mashing were pooled with the flow-through, washed with the stripping buffer, and collected by centrifugation. T cells were isolated by Naive CD4⁺ T Cell Isolation Kit (Miltenyi Biotec) in accordance with the manufacturer's instructions.

For the analysis of PP and mLN, these tissues were dissected and incubated for 1 h at 37°C in the enzymatic cocktail containing Collagenase D (1 mg/ml; Roche) and DNase I (40 U/ml; Roche) dissolved in RPMI medium supplemented with 3% FBS. The tissue was then vortexed for 10 s and passed through a 100- μ m filter. The remaining tissue was meshed on a 100- μ m cell strainer. Cells collected by mashing were pooled with the flow-through, washed with the stripping buffer, and collected by centrifugation.

For the isolation of BM, donor mice were euthanized by cervical dislocation and their femurs and tibias were dissected. Joints were cut out from the bone and the BM was isolated by

ice-cold PBS rinse. BM was collected by centrifugation, and single-cell suspension was generated by pipetting and passed through a 100- μ m filter.

Mice treatment

For the SFB colonization, freshly collected feces or cecal content of the SFB mono-associated mice were collected and frozen immediately in 50% glycerol in PBS+0.05% cysteine hydrochloride. The presence of SFB bacteria and absence of contamination was assessed by Gram-staining of the fecal smear and qPCR analysis with SFB-specific primers. Acceptor mice were fed with 50 μ l of thawed SFB suspension twice at 21 and 22 days of age. JAX and GF SFB recipient mice were moved to IsoGage bioexclusion system cages (Techniplast) and fed a sterile irradiated diet along with sterilized water. All manipulations were carried out after cage surface decontamination in a sterile hood dedicated to the IsoGage work. These mice were analyzed 2 wk later. For the IFN γ blockade, mice were i.p. injected with 250 μ g of anti-IFN γ antibody (XMGI.2; BioLegend) or the same amount of isotype control in 100 μ l of PBS. For injection and analysis time points, please see respective figure legends. For the NK/NKT cell depletion, mice were i.p. injected with 25 μ g of Nk1.1 antibody (PK136; BioXcell) at 21, 23, 25, 29, 31, and 33 days of age and analyzed at 35 days of age. For the inducible MHCII depletion on IECs, *Vil1-CreER* \times *MHCII-fl/fl* mice were i.p. injected with 1 mg of tamoxifen (Sigma-Aldrich) in 50 μ l of sunflower oil at 21 and 22 days of age. For the adoptive transfer of T cells, mice were intravenously (i.v.) injected with 5×10^6 of purified CD4⁺ T cells in 100 μ l of sterile PBS. These mice were analyzed 2 wk later. For the generation of BM chimeras, the recipient mice were irradiated (6 Gy, X-RAD 225XL; Accela) and i.v. injected with 10^7 donor BM cells in 100 μ l of PBS. To ensure better survival of recipients, they were maintained on gentamycin (1 mg/ml) in drinking water for a week after irradiation. After antibiotics treatment, recipient mice were fed with 50 μ l of thawed SFB suspension 1 and 2 days after the termination of antibiotics treatment. These mice were analyzed 4–6 wk after the irradiation. For the analysis of epithelial turnover, mice were i.p. injected with EdU (1.25 mg/mouse) in 100 μ l of PBS 72 h before the analysis.

Flow cytometry

Cells were incubated in the antibody cocktail in the stripping buffer (HBSS without Ca²⁺ and Mg²⁺ supplemented with 3% FBS and 2 mM EDTA) for 20 min on ice, washed, and either directly analyzed by flow cytometry or processed further for intracellular staining. For the staining of intracellular epitopes, cells were fixed using Foxp3/Transcription Factor Staining Buffer Set (Invitrogen) for 30 min and stained with the cocktail of antibodies at room temperature in the Foxp3 staining kit permeabilization buffer for 30 min. For the staining of cytokines and granzymes, cells were incubated in the stimulation cocktail (phorbol myristate acetate [20 ng/ml; Sigma-Aldrich], ionomycin [1 μ g/ml; Sigma-Aldrich], and Brefeldin A [10 μ g/ml; Invitrogen] in RPMI supplemented with 3% FBS) for 3–4 h at 37°C prior to the antibody staining. For the discrimination of live cells, Hoechst33258 or Fixable Viability Dye eFluo 506

(eBioscience) was used. Samples were analyzed using LSRII or Symphony FACS flow cytometers (both BD Biosciences). Flow cytometry-based cell sorting was done using FACSaria IIu cell sorter (BD Biosciences). Flow cytometry data were analyzed using FlowJO software (v10.8.1; BD Biosciences).

Fluorescence microscopy

SI tissues were dissected, and luminal contents were washed with ice-cold PBS by syringe. Tissues were then fixed in 4% formaldehyde for 2 h at room temperature. Cryoprotection was performed by incubation in 30% sucrose in PBS overnight at 4°C. Tissues were submerged in optimal cutting temperature compound medium (Agar Scientific) and snap-frozen on dry ice. Frozen tissues were stored at –80°C and cut into 12- μ m sections using CM1950 cryostat (Leica). For the EdU staining on microscopic sections, frozen sections were allowed to come to room temperature, washed three times with PBS, and blocked with 5% BSA in 0.1% Triton in PBS. After that, the manufacturer's protocol was followed using Click-iT EdU Flow Cytometry Assay Kit A488 (Life Technologies).

qPCR analysis

qPCR was used for the routine screening of SFB presence. For this analysis, bacterial DNA was isolated either from feces or from 1 cm of mouse terminal ileum using QIAmp Fast DNA Stool kit (QIAGEN). qPCR was performed using SYBR Green I qPCR Master mix on LC480II Light cycler (Both Roche). The following primers were used for this analysis: SFB (forward [F]: 5'-GAC GCTGAGGCATGAGAGCAT-3', reverse [R]: 5'-GACGGCAGGAT TGTTATTCA-3'), universal bacterial probe (F: 5'-ACTCCTACG GGAGGCAGCAGT-3', R: 5'-ATTACCGCGGCTGCTGGC-3') (Yin et al., 2013). A water sample instead of the bacterial sample was used as a negative control. The relative abundance of SFB was calculated using the relative quantification method (Pfaffl, 2001). In SFB monoisolates, as well as in SFB monocolonized mice, SFB abundance was always equal to 1. In SFB-positive mice with complex microbiota, SFB abundance ranged from $\sim 10^{-5}$ to 10^{-2} . In SFB-free mice, the reaction with SFB primers formed no valid PCR product.

For the analysis of gene expression in FACS-sorted cells, 5,000 cells were sorted directly into RLT buffer supplemented with 2-mercaptoethanol, and RNA was immediately isolated by RNeasy micro kit (Qiagen). Reverse transcription was performed using Revert Aid RT polymerase (Thermo Fisher Scientific). qPCR was performed using SYBR green master mix and LC480II light thermal cycler (both Roche). Relative expression was calculated using the relative quantification method (Pfaffl, 2001). *Cac3* gene (F: 5'-TTCGAGGTGTGCCTAACCA-3', R: 5'-GCTTAGCTCGACCACTCTGG-3') was used as the house-keeping control. Following primer pairs were used to analyze enterocyte or TA/ISC marker genes: *Apoa1* (F: 5'-GAACGAGTACCACACCAG GG-3', R: 5'-CATCAGACTATGGCGCAGGT-3'), *Fabp1* (F: 5'-AGC CAGGAGAACCTTTGAGCC-3', R: 5'-CACCCCTTGATGTCCTTCC-3'), *Lgr5* (F: 5'-CTGCCCATCACACTGTCACT-3', R: 5'-GCAGAG GCGATGTAGGAGAC-3'), and *Olfm4* (F: 5'-ATGACAGAAAGG ACGCTGGG-3', R: 5'-ACACAGGTTTCAGGAGCCAG-3').

Organoid culture

Freshly isolated SI crypts were used as the input for the organoid culture. Crypts were counted and 90 crypts per well were used. Crypts were collected by centrifugation (300 g, 1 min, 4°C) and resuspended in 100 μ l of Matrigel (Corning) per well. Matrigel with the crypts was plated on 24-well plates in three droplets per well. Matrigel was left to solidify at 37°C for 5 min and overlaid by organoid culture media. Organoid culture media was prepared from DMEM/F12 (Thermo Fisher Scientific) supplemented with GlutaMax (Thermo Fisher Scientific), HEPES (Thermo Fisher Scientific), penicillin/streptomycin (Thermo Fisher Scientific), N2 supplement (Thermo Fisher Scientific), B27 supplement (Thermo Fisher Scientific), N-acetylcysteine (Sigma-Aldrich), mNoggin (PeproTech), mEGF (Thermo Fisher Scientific), and Rspo1 (PeproTech). The medium was exchanged on the third day of culture. On the fourth day of culture, IFN γ (final concentration, 10 ng/ml; ImmunoTools) and SFB-derived peptide cognate for SFBtg T cells (custom peptide synthesis, final concentration, 1 ng/ml; Thermo Fisher Scientific) were added to the culture media. On the fifth day of culture, organoids were harvested and cultured for 1 h in organoid culture media supplemented with IFN γ and SFB peptide, together with freshly isolated IEL from SFB-colonized SFBtg mice in 5:1 ratio (organoid cells:IEL). Cells were then harvested, plated in Matrigel, and cultured in organoid culture media supplemented with IFN γ and SFB peptide for 48 h. All culturing steps were done at 37°C in a humidified thermal incubator. Finally, organoids were harvested, digested in TrypLE express (Thermo Fisher Scientific) for 1 min at 37°C, and used for FACS analysis. Wells that contained <2,000 cells were excluded from the analysis.

scRNA-seq

For the droplet-based scRNA-seq, freshly isolated cells were FACS-sorted using CD45, EpCAM, and Hoechst33258 staining. LP and IEL cells were sorted as live CD45⁺ cells, whereas epithelial cells were sorted as EpCAM⁺ CD45⁻ live cells. SI-IECs and SI-IEL from JAX and SFB-colonized JAX mice were isolated and sorted separately, but cells from each mouse were pooled before the 10 \times sequencing pipeline. Separation of IECs from LP/IEL cells was performed bioinformatically based on the combination of UMAP clustering and canonic hematopoietic (*Ptprc*) and epithelial (*Epcam*) marker genes. SI-LP cells from JAX and SFB colonized JAX mice cells were processed separately. SI-LP, SI-IEL, and SI-IEC cells from JAX and SFB colonized JAX mice were processed in one experiment, including cell preparation, sorting, droplets generation, and sequencing.

The viability of cells was assessed by trypan blue and counted in an automated TC20 cell counter (Bio-Rad) prior to library preparation. scRNA-seq libraries were prepared using Chromium controller instrument and Chromium Next Gem single-cell 3' reagent kit version 3.1 (both 10X Genomics) in accordance with the manufacturer's protocol. The quality and quantity of the resulting cDNA and libraries were determined using Agilent 2100 Bioanalyzer (Agilent Technologies). The libraries were sequenced using NextSeq 500 instrument (Illumina) in accordance with the manufacturer's protocol with an mRNA fragment read length of 54 bases. We used 10X Genomics Cell Ranger

software suite (version 4.0.0) to quantify gene-level expression based on GRCh38 assembly (Ensembl annotation version 98) (Cunningham et al., 2019).

Well-based scRNA-seq was done using SORT-Seq platform (Muraro et al., 2016). Freshly isolated SI-LP and SI-IEL cells (as described above) were stained with antibodies recognizing TCR β , CD4, CD8 α , CD8 β , CD90.1, CD90.2, and V β 14 subunit of TCR. SFBtg T cells were sorted as live TCR β ⁺ CD90.1⁺ V β 14⁺ cells. Host cells were sorted as live TCR β ⁺ cells. All the markers were recorded while sorting and later integrated with scRNA-seq data using indexes generated during cell sorting. Cells were sorted into 384-well plates (provided by Single Cell Discoveries) and snap-frozen on dry ice straight after sorting. The CEL-Seq2 protocol was used for library preparation by Single Cell Discoveries (Muraro et al., 2016). The libraries were sequenced using NextSeq 500 instrument (Illumina) in accordance with the manufacturer's protocol.

Bioinformatic analysis

All the bioinformatic analyses were done using R (version 4.1.1). For the analysis of droplet-based scRNA-seq datasets, 10 \times pipeline was used to generate read-count matrices. This data served as an input for all the downstream analyses. First, the ambient RNA was removed using SoupX R package (v 1.5.2). Cells that contained >5% of mitochondrial RNA from their total mapped reads were removed. This step was followed by the separation of IECs from IEL cells which were sequenced together. For this UMAP clustering and the expression of canonic hematopoietic (*Ptprc*) and epithelial (*Epcam*) marker genes, was used to identify the hematopoietic and epithelial cells. Thus, cells of hematopoietic or epithelial origin were defined, separated, and processed separately in all downstream analyses. Further data processing was done using the standard Seurat R package (v 4.0.4) pipeline. Briefly, cells were clustered, and their cell types were annotated based on canonic markers. When a cluster contained a mixed population, this approach was repeated and the cluster was further subdivided into populations representing unique cell types. Thus, we identified cell types, which served as the main components for further downstream analysis. Similar to droplet-based scRNA-seq datasets, we processed plate-based scRNA-seq datasets by a standard Seurat R package (v 4.0.4) pipeline.

Statistics

Aside from sequencing datasets, all the remaining data were tested using GraphPad Prism 9.

Online supplemental material

Fig. S1 shows the representative FACS gating for SI-IEC, SI-LP, and the SFB levels after acute and chronic colonization. Fig. S2 shows representative FACS gating of IFN γ -expressing cell analysis, cell-specific targeting validation, and scRNA-seq analysis of SI-IEC from JAX and JAX + SFB mice. Fig. S3 shows the analysis of SI-IEL after SFB colonization and their dependence on epithelial MHCII. Fig. S4 shows the analysis of SFB-specific T cell response in the SI. Fig. S5 shows the protocol for FACS-based analysis of enterocytes.

Data availability

Sequencing data are available on the European Bioinformatics Institute Array Express portal under the accession code E-MTAB-12391. The additional data pertaining to this study are available from the corresponding authors upon reasonable request.

Acknowledgments

We are thankful to Martina Krausová and Šárka Kocourková from the Genomics and Bioinformatics core facility of the Institute of Molecular Genetics in Prague, Czech Republic, for the preparation of single-cell libraries and to Zdeněk Cimburek from the Flow Cytometry Core Facility of the Institute of Molecular Genetics in Prague, Czech Republic for suggestions related to cell sorting. We thank the Animal Facility in Krč personnel of the Institute of Molecular Genetics in Prague, Czech Republic for their excellent maintenance of our animal colonies and Šárka Maisnerová from the Laboratory of Gnotobiology, Institute of Microbiology in Nový Hrádek, Czech Republic for the GF and SFB-negative mice maintenance. We are thankful to Bernard Malissen (Centre d'Immunologie de Marseille Luminy, Marseille, France), Ulrich Kalinke (Helmholtz Centre for Infection Research, Hannover, Germany), and Veronika Sexl (Veterinary University of Vienna, Vienna, Austria) for valuable mouse strains.

Research in the Dobeš laboratory (J. Dobeš, T. Brabec, K. Kováčová, M. Dobešová, I. Pacáková) is kindly supported by the Czech Science Foundation JUNIOR STAR grant (no. 21-22435M), Czech Science Foundation grant (no. 22-30879S) and by Charles University PRIMUS grant (no. Primus/21/MED/003). M. Schwarzer and D. Šrůtková are supported by the Czech Science Foundation JUNIOR STAR grant (no. 21-19640M). D. Filipp, I. Šplichalová, and J. Březina are supported by grant no. 20-30350S and 22-30879S from the Czech Science Foundation. M. Kolář is supported by the Operational Programme Research, Development and Education project (no. CZ.02.1.01/0.0/0.0/16_019/0000785).

Author contributions: T. Brabec, D. Filipp, J. Abramson, and J. Dobeš initiated the project. T. Brabec and J. Dobeš designed the vast majority of experiments, critically discussed the data, and wrote and revised the manuscript in close collaboration. T. Brabec executed and analyzed the majority of the experiments, J. Dobeš executed some of the experiments and acquired the funding. J. Abramson and D. Filipp critically discussed the results, revised the manuscript, and contributed with critically important reagents. M. Schwarzer critically contributed to the design of gnotobiotic experiments and together with D. Šrůtková provided SFB monoisolates, performed all SFB colonization experiments and handled all gnotobiotic animals. K. Kováčová performed majority of microscopy analysis and provided technical support for the project. M. Dobešová performed some of the experiments, carried out the majority of mouse genotyping, and provided technical support for the project. J. Březina performed animal irradiation, critically discussed the data and the manuscript. I. Pacáková provided support in some of the experiments. D. Schierová, O. Ben-Nun, Y. Goldfarb, and I. Šplichalová

performed some of the experiments. M. Kolář provided technical expertise in scRNA-seq experiments.

Disclosures: The authors declare no competing interests exist.

Submitted: 1 February 2023

Revised: 16 August 2023

Accepted: 9 October 2023

References

- Al Nabhani, Z., S. Dulauroy, R. Marques, C. Cousu, S. Al Bounny, F. Déjardin, T. Sparwasser, M. Bérard, N. Cerf-Bensussan, and G. Eberl. 2019. A weaning reaction to microbiota is required for resistance to immunopathologies in the adult. *Immunity*. 50:1276–1288.e5. <https://doi.org/10.1016/j.immuni.2019.02.014>
- Arnaud-Battandier, F., N. Cerf-Bensussan, R. Amsellem, and J. Schmitz. 1986. Increased HLA-DR expression by enterocytes in children with celiac disease. *Gastroenterology*. 91:1206–1212. [https://doi.org/10.1016/S0016-5085\(86\)80018-X](https://doi.org/10.1016/S0016-5085(86)80018-X)
- Atarashi, K., T. Tanoue, M. Ando, N. Kamada, Y. Nagano, S. Narushima, W. Suda, A. Imaoka, H. Setoyama, T. Nagamori, et al. 2015. Th17 cell induction by adhesion of microbes to intestinal epithelial cells. *Cell*. 163:367–380. <https://doi.org/10.1016/j.cell.2015.08.058>
- Bevins, C.L., and N.H. Salzman. 2011. Paneth cells, antimicrobial peptides and maintenance of intestinal homeostasis. *Nat. Rev. Microbiol.* 9:356–368. <https://doi.org/10.1038/nrmicro2546>
- Beyaz, S., C. Chung, H. Mou, K.E. Bauer-Rowe, M.E. Xifaras, I. Ergin, L. Dohnalova, M. Biton, K. Shekhar, O. Eskioçak, et al. 2021. Dietary suppression of MHC class II expression in intestinal epithelial cells enhances intestinal tumorigenesis. *Cell Stem Cell*. 28:1922–1935.e5. <https://doi.org/10.1016/j.stem.2021.08.007>
- Bilate, A.M., D. Bousbaine, L. Mesin, M. Agudelo, J. Leube, A. Kratzert, S.K. Dougan, G.D. Victora, and H.L. Ploegh. 2016. Tissue-specific emergence of regulatory and intraepithelial T cells from a clonal T cell precursor. *Sci. Immunol.* 1:eaa7471. <https://doi.org/10.1126/sciimmunol.aaf7471>
- Bilate, A.M., M. London, T.B.R. Castro, L. Mesin, J. Bortolatto, S. Kongthong, A. Harnagel, G.D. Victora, and D. Mucida. 2020. T cell receptor is required for differentiation, but not maintenance, of intestinal CD4⁺ intraepithelial lymphocytes. *Immunity*. 53:1001–1014.e20. <https://doi.org/10.1016/j.immuni.2020.09.003>
- Biton, M., A.L. Haber, N. Rogel, G. Burgin, S. Beyaz, A. Schnell, O. Ashenberg, C.W. Su, C. Smillie, K. Shekhar, et al. 2018. T helper cell cytokines modulate intestinal stem cell renewal and differentiation. *Cell*. 175:1307–1320.e22. <https://doi.org/10.1016/j.cell.2018.10.008>
- Blumershteyn, R.V., and D.C. Savage. 1977. Filamentous microbes indigenous to the murine small bowel: A scanning electron microscopic study of their morphology and attachment to the epithelium. *Microb. Ecol.* 4:95–103. <https://doi.org/10.1007/BF02014280>
- Borst, K., S. Flindt, P. Blank, P.K. Larsen, C. Chhatbar, J. Skerra, J. Spanier, C. Hirche, M. König, T. Alantalo, et al. 2020. Selective reconstitution of IFN- γ gene function in Ncr1⁺ NK cells is sufficient to control systemic vaccinia virus infection. *PLoS Pathog.* 16:e1008279. <https://doi.org/10.1371/journal.ppat.1008279>
- Bousbaine, D., L.I. Fisch, M. London, P. Bhagchandani, T.B. Rezende de Castro, M. Mimee, S. Olesen, B.S. Reis, D. VanInsberghe, J. Bortolatto, et al. 2022. A conserved Bacteroidetes antigen induces anti-inflammatory intestinal T lymphocytes. *Science*. 377:660–666. <https://doi.org/10.1126/science.abg5645>
- Ceppek, K.L., S.K. Shaw, C.M. Parker, G.J. Russell, J.S. Morrow, D.L. Rimm, and M.B. Brenner. 1994. Adhesion between epithelial cells and T lymphocytes mediated by E-cadherin and the alpha E beta 7 integrin. *Nature*. 372:190–193. <https://doi.org/10.1038/372190a0>
- Cervantes-Barragan, L., J.N. Chai, M.D. Tianero, B. Di Luccia, P.P. Ahern, J. Merriman, V.S. Cortez, M.G. Caparon, M.S. Donia, S. Gillfillan, et al. 2017. Lactobacillus reuteri induces gut intraepithelial CD4⁺CD8 $\alpha\alpha$ ⁺ T cells. *Science*. 357:806–810. <https://doi.org/10.1126/science.aah5825>
- Chardès, T., D. Buzoni-Gatel, A. Lepage, F. Bernard, and D. Bout. 1994. Toxoplasma gondii oral infection induces specific cytotoxic CD8 alpha/beta⁺ Thy-1⁺ gut intraepithelial lymphocytes, lytic for parasite-infected enterocytes. *J. Immunol.* 153:4596–4603. <https://doi.org/10.4049/jimmunol.153.10.4596>

- Cheroutre, H., F. Lambomez, and D. Mucida. 2011. The light and dark sides of intestinal intraepithelial lymphocytes. *Nat. Rev. Immunol.* 11:445–456. <https://doi.org/10.1038/nri3007>
- Collins, J.W., K.M. Keeney, V.F. Crepin, V.A.K. Rathinam, K.A. Fitzgerald, B.B. Finlay, and G. Frankel. 2014. Citrobacter rodentium: Infection, inflammation and the microbiota. *Nat. Rev. Microbiol.* 12:612–623. <https://doi.org/10.1038/nrmiicro3315>
- Cunningham, F., P. Achuthan, W. Akanni, J. Allen, M.R. Amode, I.M. Armean, R. Bennett, J. Bhai, K. Billis, S. Boddu, et al. 2019. Ensembl 2019. *Nucleic Acids Res.* 47:D745–D751. <https://doi.org/10.1093/nar/gky1113>
- Eckelhart, E., W. Warsch, E. Zebedin, O. Simma, D. Stoiber, T. Kolbe, T. Rüllicke, M. Mueller, E. Casanova, and V. Sexl. 2011. A novel Nrcl-Cre mouse reveals the essential role of STAT5 for NK-cell survival and development. *Blood.* 117:1565–1573. <https://doi.org/10.1182/blood-2010-06-291633>
- el Marjou, F., K.P. Janssen, B.H.J. Chang, M. Li, V. Hindie, L. Chan, D. Louvard, P. Chambon, D. Metzger, and S. Robine. 2004. Tissue-specific and inducible Cre-mediated recombination in the gut epithelium. *Genesis.* 39:186–193. <https://doi.org/10.1002/gene.20042>
- Farkas, A.M., C. Panea, Y. Goto, G. Nakato, M. Galan-Diez, S. Narushima, K. Honda, and I.I. Ivanov. 2015. Induction of Th17 cells by segmented filamentous bacteria in the murine intestine. *J. Immunol. Methods.* 421:104–111. <https://doi.org/10.1016/j.jim.2015.03.020>
- Flannigan, K.L., V.L. Ngo, D. Geem, A. Harusato, A. Hirota, C.A. Parkos, N.W. Lukacs, A. Nusrat, V. Gaboriau-Routhiau, N. Cerf-Bensussan, et al. 2017. IL-17A-mediated neutrophil recruitment limits expansion of segmented filamentous bacteria. *Mucosal Immunol.* 10:673–684. <https://doi.org/10.1038/mi.2016.80>
- Gaboriau-Routhiau, V., S. Rakotobe, E. Lécuyer, I. Mulder, A. Lan, C. Bridonneau, V. Rochet, A. Pisi, M. De Paepe, G. Brandi, et al. 2009. The key role of segmented filamentous bacteria in the coordinated maturation of gut helper T cell responses. *Immunity.* 31:677–689. <https://doi.org/10.1016/j.immuni.2009.08.020>
- Glaser, A., A. Levi, J. Enk, B. Isaacson, S. Viukov, S. Orlanski, A. Scope, T. Neuman, C.D. Enk, J.H. Hanna, et al. 2018. Nkp46 receptor-mediated interferon- γ production by natural killer cells increases fibronectin 1 to alter tumor architecture and control metastasis. *Immunity.* 48:107–119.e4. <https://doi.org/10.1016/j.immuni.2017.12.007>
- Gorvel, J.P., J. Sarles, S. Maroux, D. Olive, and C. Mawas. 1984. Cellular localization of class I (HLA-A, B, C) and class II (HLA-DR and DQ) MHC antigens on the epithelial cells of normal human jejunum. *Biol. Cell.* 52:249–252. <https://doi.org/10.1111/j.1768-322X.1985.tb00343.x>
- Goto, Y., C. Panea, G. Nakato, A. Cebula, C. Lee, M.G. Diez, T.M. Laufer, L. Ignatowicz, and I.I. Ivanov. 2014. Segmented filamentous bacteria antigens presented by intestinal dendritic cells drive mucosal Th17 cell differentiation. *Immunity.* 40:594–607. <https://doi.org/10.1016/j.immuni.2014.03.005>
- Haber, A.L., M. Biton, N. Rogel, R.H. Herbst, K. Shekhar, C. Smillie, G. Burgin, T.M. Delorey, M.R. Howitt, Y. Katz, et al. 2017. A single-cell survey of the small intestinal epithelium. *Nature.* 551:333–339. <https://doi.org/10.1038/nature24489>
- Hashimoto, K., S.K. Joshi, and P.A. Koni. 2002. A conditional null allele of the major histocompatibility IA-beta chain gene. *Genesis.* 32:152–153. <https://doi.org/10.1002/gene.10056>
- Hayday, A., E. Theodoridis, E. Ramsburg, and J. Shires. 2001. Intraepithelial lymphocytes: Exploring the third way in immunology. *Nat. Immunol.* 2:997–1003. <https://doi.org/10.1038/ni1101-997>
- He, X., X. He, V.P. Dave, Y. Zhang, X. Hua, E. Nicolas, W. Xu, B.A. Roe, and D.J. Kappes. 2005. The zinc finger transcription factor Th-POK regulates CD4 versus CD8 T-cell lineage commitment. *Nature.* 433:826–833. <https://doi.org/10.1038/nature03338>
- Heuberger, C.E., A. Janney, N. Ilott, A. Bertocchi, S. Pott, Y. Gu, M. Pohin, M. Friedrich, E.H. Mann, C. Pearson, et al. 2023. MHC class II antigen presentation by intestinal epithelial cells fine-tunes bacteria-reactive CD4 T cell responses. *Mucosal Immunol.* S1933–0219(23)00032–6. <https://doi.org/10.1016/j.mucimm.2023.05.001>
- Ivanov, I.I., K. Atarashi, N. Manel, E.L. Brodie, T. Shima, U. Karaoz, D. Wei, K.C. Goldfarb, C.A. Santee, S.V. Lynch, et al. 2009. Induction of intestinal Th17 cells by segmented filamentous bacteria. *Cell.* 139:485–498. <https://doi.org/10.1016/j.cell.2009.09.033>
- Ivanov, I.I., R.d. L. Frutos, N. Manel, K. Yoshinaga, D.B. Rifkin, R.B. Sartor, B.B. Finlay, and D.R. Littman. 2008. Specific microbiota direct the differentiation of IL-17-producing T-helper cells in the mucosa of the small intestine. *Cell Host Microbe.* 4:337–349. <https://doi.org/10.1016/j.chom.2008.09.009>
- Ivanov, I.I., and D.R. Littman. 2010. Segmented filamentous bacteria take the stage. *Mucosal Immunol.* 3:209–212. <https://doi.org/10.1038/mi.2010.3>
- Jamwal, D.R., D. Laubitz, C.A. Harrison, V. Figliuolo da Paz, C.M. Cox, R. Wong, M. Midura-Kiela, M.A. Gurney, D.G. Besselsen, P. Setty, et al. 2020. Intestinal epithelial expression of MHCII determines severity of chemical, T-cell-induced, and infectious colitis in mice. *Gastroenterology.* 159:1342–1356.e6. <https://doi.org/10.1053/j.gastro.2020.06.049>
- Kilshaw, P.J., and S.J. Murant. 1990. A new surface antigen on intraepithelial lymphocytes in the intestine. *Eur. J. Immunol.* 20:2201–2207. <https://doi.org/10.1002/eji.1830201008>
- Klaasen, H.L., J.P. Koopman, F.G. Poelma, and A.C. Beynen. 1992. Intestinal, segmented, filamentous bacteria. *FEMS Microbiol. Rev.* 8:165–180. <https://doi.org/10.1111/j.1574-6968.1992.tb04986.x>
- Koyama, M., P. Mukhopadhyay, I.S. Schuster, A.S. Henden, J. Hülsdünker, A. Varelias, M. Vetizou, R.D. Kuns, R.J. Robb, P. Zhang, et al. 2019. MHC class II antigen presentation by the intestinal epithelium initiates graft-versus-host disease and is influenced by the microbiota. *Immunity.* 51:885–898.e7. <https://doi.org/10.1016/j.immuni.2019.08.011>
- Kumar, P., L. Monin, P. Castillo, W. Elsegeiny, W. Horne, T. Eddens, A. Vikram, M. Good, A.A. Schoenborn, K. Bibby, et al. 2016. Intestinal interleukin-17 receptor signaling mediates reciprocal control of the gut microbiota and autoimmune inflammation. *Immunity.* 44:659–671. <https://doi.org/10.1016/j.immuni.2016.02.007>
- Ladinsky, M.S., L.P. Araujo, X. Zhang, J. Veltri, M. Galan-Diez, S. Soualhi, C. Lee, K. Irie, E.Y. Pinker, S. Narushima, et al. 2019. Endocytosis of commensal antigens by intestinal epithelial cells regulates mucosal T cell homeostasis. *Science.* 363:eaat4042. <https://doi.org/10.1126/science.aat4042>
- Lecuyer, E., S. Rakotobe, H. Lengline-Garnier, C. Lebreton, M. Picard, C. Juste, R. Fritzen, G. Eberl, K.D. McCoy, A.J. Macpherson, et al. 2014. Segmented filamentous bacterium uses secondary and tertiary lymphoid tissues to induce gut IgA and specific T helper 17 cell responses. *Immunity.* 40:608–620. <https://doi.org/10.1016/j.immuni.2014.03.009>
- Lee, P.P., D.R. Fitzpatrick, C. Beard, H.K. Jessup, S. Lehar, K.W. Makar, M. Pérez-Melgosa, M.T. Sweetser, M.S. Schlissel, S. Nguyen, et al. 2001. A critical role for Dnmt1 and DNA methylation in T cell development, function, and survival. *Immunity.* 15:763–774. [https://doi.org/10.1016/S1074-7613\(01\)00227-8](https://doi.org/10.1016/S1074-7613(01)00227-8)
- Leishman, A.J., O.V. Naidenko, A. Attinger, F. Koning, C.J. Lena, Y. Xiong, H.C. Chang, E. Reinherz, M. Kronenberg, and H. Cheroutre. 2001. T cell responses modulated through interaction between CD8 α and the nonclassical MHC class I molecule, TL. *Science.* 294:1936–1939. <https://doi.org/10.1126/science.1063564>
- Lepage, A.C., D. Buzoni-Gatel, D.T. Bout, and L.H. Kasper. 1998. Gut-derived intraepithelial lymphocytes induce long term immunity against *Toxoplasma gondii*. *J. Immunol.* 161:4902–4908. <https://doi.org/10.4049/jimmunol.161.9.4902>
- Lockhart, A., A. Reed, T. Rezende de Castro, C. Herman, M.C. Campos Cansoso, and D. Mucida. 2023. Dietary protein shapes the profile and repertoire of intestinal CD4 $^{+}$ T cells. *J. Exp. Med.* 220:e20221816. <https://doi.org/10.1084/jem.20221816>
- Maloy, K.J., and F. Powrie. 2011. Intestinal homeostasis and its breakdown in inflammatory bowel disease. *Nature.* 474:298–306. <https://doi.org/10.1038/nature10208>
- Masopust, D., V. Vezys, E.J. Wherry, D.L. Barber, and R. Ahmed. 2006. Cutting edge: Gut microenvironment promotes differentiation of a unique memory CD8 T cell population. *J. Immunol.* 176:2079–2083. <https://doi.org/10.4049/jimmunol.176.4.2079>
- Mombaerts, P., J. Arnoldi, F. Russ, S. Tonegawa, and S.H. Kaufmann. 1993. Different roles of alpha beta and gamma delta T cells in immunity against an intracellular bacterial pathogen. *Nature.* 365:53–56. <https://doi.org/10.1038/365053a0>
- Mombaerts, P., J. Iacomini, R.S. Johnson, K. Herrup, S. Tonegawa, and V.E. Papaioannou. 1992. RAG-1-deficient mice have no mature B and T lymphocytes. *Cell.* 68:869–877. [https://doi.org/10.1016/0092-8674\(92\)90030-G](https://doi.org/10.1016/0092-8674(92)90030-G)
- Moon, S., Y. Park, S. Hyeon, Y.M. Kim, J.H. Kim, H. Kim, S. Park, K.J. Lee, B.K. Koo, S.J. Ha, and S.W. Lee. 2021. Niche-specific MHC II and PD-L1 regulate CD4 $^{+}$ CD8 $\alpha\alpha^{+}$ intraepithelial lymphocyte differentiation. *J. Exp. Med.* 218:e20201665. <https://doi.org/10.1084/jem.20201665>
- Mucida, D., M.M. Husain, S. Muroi, F. van Wijk, R. Shinnakasu, Y. Naoe, B.S. Reis, Y. Huang, F. Lambomez, M. Docherty, et al. 2013. Transcriptional reprogramming of mature CD4 $^{+}$ helper T cells generates distinct MHC class II-restricted cytotoxic T lymphocytes. *Nat. Immunol.* 14:281–289. <https://doi.org/10.1038/ni.2523>

- Muraro, M.J., G. Dharmadhikari, D. Grün, N. Groen, T. Dielen, E. Jansen, L. van Gurp, M.A. Engelse, F. Carlotti, E.J.P. de Koning, and A. van Oudenaarden. 2016. A single-cell transcriptome atlas of the human pancreas. *Cell Syst.* 3:385–394.e3. <https://doi.org/10.1016/j.cels.2016.09.002>
- Müller, S., M. Bühler-Jungo, and C. Mueller. 2000. Intestinal intraepithelial lymphocytes exert potent protective cytotoxic activity during an acute virus infection. *J. Immunol.* 164:1986–1994. <https://doi.org/10.4049/jimmunol.164.4.1986>
- Parsa, R., M. London, T.B. Rezende de Castro, B. Reis, J. Buissant des Amorie, J.G. Smith, and D. Mucida. 2022. Newly recruited intraepithelial Ly6A⁺CCR9⁺CD4⁺ T cells protect against enteric viral infection. *Immunity.* 55:1234–1249.e6. <https://doi.org/10.1016/j.immuni.2022.05.001>
- Pfaffl, M.W. 2001. A new mathematical model for relative quantification in real-time RT-PCR. *Nucleic Acids Res.* 29:e45. <https://doi.org/10.1093/nar/29.9.e45>
- Pickert, G., C. Neufert, M. Leppkes, Y. Zheng, N. Wittkopf, M. Warntjen, H.A. Lehr, S. Hirth, B. Weigmann, S. Wirtz, et al. 2009. STAT3 links IL-22 signaling in intestinal epithelial cells to mucosal wound healing. *J. Exp. Med.* 206:1465–1472. <https://doi.org/10.1084/jem.20082683>
- Reis, B.S., A. Rogoz, F.A. Costa-Pinto, I. Taniuchi, and D. Mucida. 2013. Mutual expression of the transcription factors Runx3 and ThPOK regulates intestinal CD4⁺ T cell immunity. *Nat. Immunol.* 14:271–280. <https://doi.org/10.1038/ni.2518>
- Russler-Germain, E.V., J. Jung, A.T. Miller, S. Young, J. Yi, A. Wehmeier, L.E. Fox, K.J. Monte, J.N. Chai, D.H. Kulkarni, et al. 2021. Commensal *Cryptosporidium* colonization elicits a cDC1-dependent Th1 response that promotes intestinal homeostasis and limits other infections. *Immunity.* 54:2547–2564.e7. <https://doi.org/10.1016/j.immuni.2021.10.002>
- Sano, T., W. Huang, J.A. Hall, Y. Yang, A. Chen, S.J. Gavzy, J.Y. Lee, J.W. Ziel, E.R. Miraldi, A.I. Domingos, et al. 2015. An IL-23r/IL-22 circuit regulates epithelial serum amyloid A to promote local effector Th17 responses. *Cell.* 163:381–393. <https://doi.org/10.1016/j.cell.2015.08.061>
- Scott, H., B.G. Solheim, P. Brandtzaeg, and E. Thorsby. 1980. HLA-DR-like antigens in the epithelium of the human small intestine. *Scand. J. Immunol.* 12:77–82. <https://doi.org/10.1111/j.1365-3083.1980.tb00043.x>
- Shi, Z., J. Zou, Z. Zhang, X. Zhao, J. Noriega, B. Zhang, C. Zhao, H. Ingle, K. Bittinger, L.M. Mattei, et al. 2019. Segmented filamentous bacteria prevent and cure rotavirus infection. *Cell.* 179:644–658.e13. <https://doi.org/10.1016/j.cell.2019.09.028>
- Shih, V.F.S., J. Cox, N.M. Kljavin, H.S. Dengler, M. Reichelt, P. Kumar, L. Rangell, J.K. Kolls, L. Diehl, W. Ouyang, and N. Ghilardi. 2014. Homeostatic IL-23 receptor signaling limits Th17 response through IL-22-mediated containment of commensal microbiota. *Proc. Natl. Acad. Sci. USA.* 111:13942–13947. <https://doi.org/10.1073/pnas.1323852111>
- Shires, J., E. Theodoridis, and A.C. Hayday. 2001. Biological insights into TCR γ delta⁺ and TCR α beta⁺ intraepithelial lymphocytes provided by serial analysis of gene expression (SAGE). *Immunity.* 15:419–434. [https://doi.org/10.1016/S1074-7613\(01\)00192-3](https://doi.org/10.1016/S1074-7613(01)00192-3)
- Suzuki, K., B. Meek, Y. Doi, M. Muramatsu, T. Chiba, T. Honjo, and S. Fagarasan. 2004. Aberrant expansion of segmented filamentous bacteria in IgA-deficient gut. *Proc. Natl. Acad. Sci. USA.* 101:1981–1986. <https://doi.org/10.1073/pnas.0307317101>
- Thelemann, C., R.O. Eren, M. Coutaz, J. Brasseit, H. Bouzourene, M. Rosa, A. Duval, C. Lavanchy, V. Mack, C. Mueller, et al. 2014. Interferon- γ induces expression of MHC class II on intestinal epithelial cells and protects mice from colitis. *PLoS One.* 9:e86844. <https://doi.org/10.1371/journal.pone.0086844>
- Thompson, C.L., R. Vier, A. Mikaelyan, T. Wienemann, and A. Brune. 2012. ‘*Candidatus arthromitus*’ revised: Segmented filamentous bacteria in arthropod guts are members of lachnospiraceae. *Environ. Microbiol.* 14:1454–1465. <https://doi.org/10.1111/j.1462-2920.2012.02731.x>
- Tuganbaev, T., U. Mor, S. Bashiardes, T. Liwinski, S.P. Nobs, A. Leshem, M. Dori-Bachash, C.A. Thaiss, E.Y. Pinker, K. Ratiner, et al. 2020. Diet diurnally regulates small intestinal microbiome-epithelial-immune homeostasis and enteritis. *Cell.* 182:1441–1459.e21. <https://doi.org/10.1016/j.cell.2020.08.027>
- Umesaki, Y., Y. Okada, S. Matsumoto, A. Imaoka, and H. Setoyama. 1995. Segmented filamentous bacteria are indigenous intestinal bacteria that activate intraepithelial lymphocytes and induce MHC class II molecules and fucosyl asialo GM1 glycolipids on the small intestinal epithelial cells in the ex-germ-free mouse. *Microbiol. Immunol.* 39:555–562. <https://doi.org/10.1111/j.1348-0421.1995.tb02242.x>
- Van Der Kraak, L.A., C. Schneider, V. Dang, A.H.P. Burr, E.S. Weiss, J.A. Varghese, L. Yang, T.W. Hand, and S.W. Canna. 2021. Genetic and commensal induction of IL-18 drive intestinal epithelial MHCII via IFN γ . *Mucosal Immunol.* 14:1100–1112. <https://doi.org/10.1038/s41385-021-00419-1>
- Voehringer, D., H.E. Liang, and R.M. Locksley. 2008. Homeostasis and effector function of lymphopenia-induced “memory-like” T cells in constitutively T cell-depleted mice. *J. Immunol.* 180:4742–4753. <https://doi.org/10.4049/jimmunol.180.7.4742>
- Wiles, S., W.P. Hanage, G. Frankel, and B. Robertson. 2006. Modelling infectious disease: Time to think outside the box? *Nat. Rev. Microbiol.* 4:307–312. <https://doi.org/10.1038/nrmicro1386>
- Wohn, C., V. Le Guen, O. Voluzan, F. Fiore, S. Henri, and B. Malissen. 2020. Absence of MHC class II on cDC1 dendritic cells triggers fatal autoimmunity to a cross-presented self-antigen. *Sci. Immunol.* 5:eaba1896. <https://doi.org/10.1126/sciimmunol.aba1896>
- Yang, Y., M.B. Torchinsky, M. Gobert, H. Xiong, M. Xu, J.L. Linehan, F. Alonzo, C. Ng, A. Chen, X. Lin, et al. 2014. Focused specificity of intestinal Th17 cells towards commensal bacterial antigens. *Nature.* 510:152–156. <https://doi.org/10.1038/nature13279>
- Yin, Y., Y. Wang, L. Zhu, W. Liu, N. Liao, M. Jiang, B. Zhu, H.D. Yu, C. Xiang, and X. Wang. 2013. Comparative analysis of the distribution of segmented filamentous bacteria in humans, mice and chickens. *ISME J.* 7:615–621. <https://doi.org/10.1038/ismej.2012.128>

Supplemental material

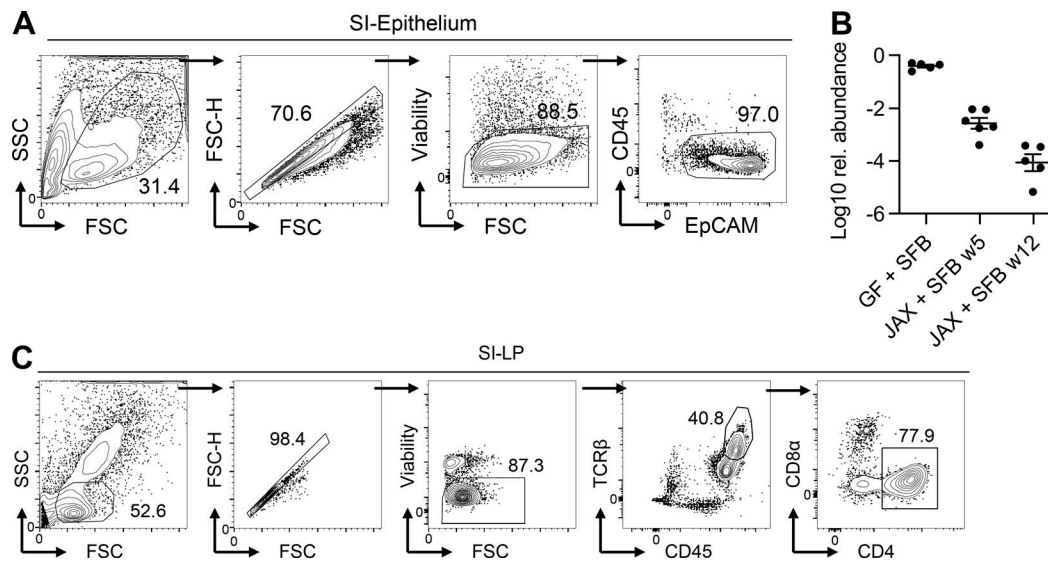


Figure S1. **Representative FACS gating for SI-IEC, SI-LP, and levels of SFB in acute and chronic colonization. (A)** Basic gating for the FACS analysis of SI epithelium. Numbers beside gates represent frequencies from the parent gate. **(B)** qPCR analysis of SFB levels relative to all bacteria using primers specific for SFB 16S and universal 16S primers. Data are shown as \log_{10} of relative abundance. Two independent experiments, $n = 5-6$. Lines show mean \pm SEM. **(C)** Basic gating for the FACS analysis of SI-LP CD4⁺ T cells. Numbers beside gates represent frequencies from parent gate.

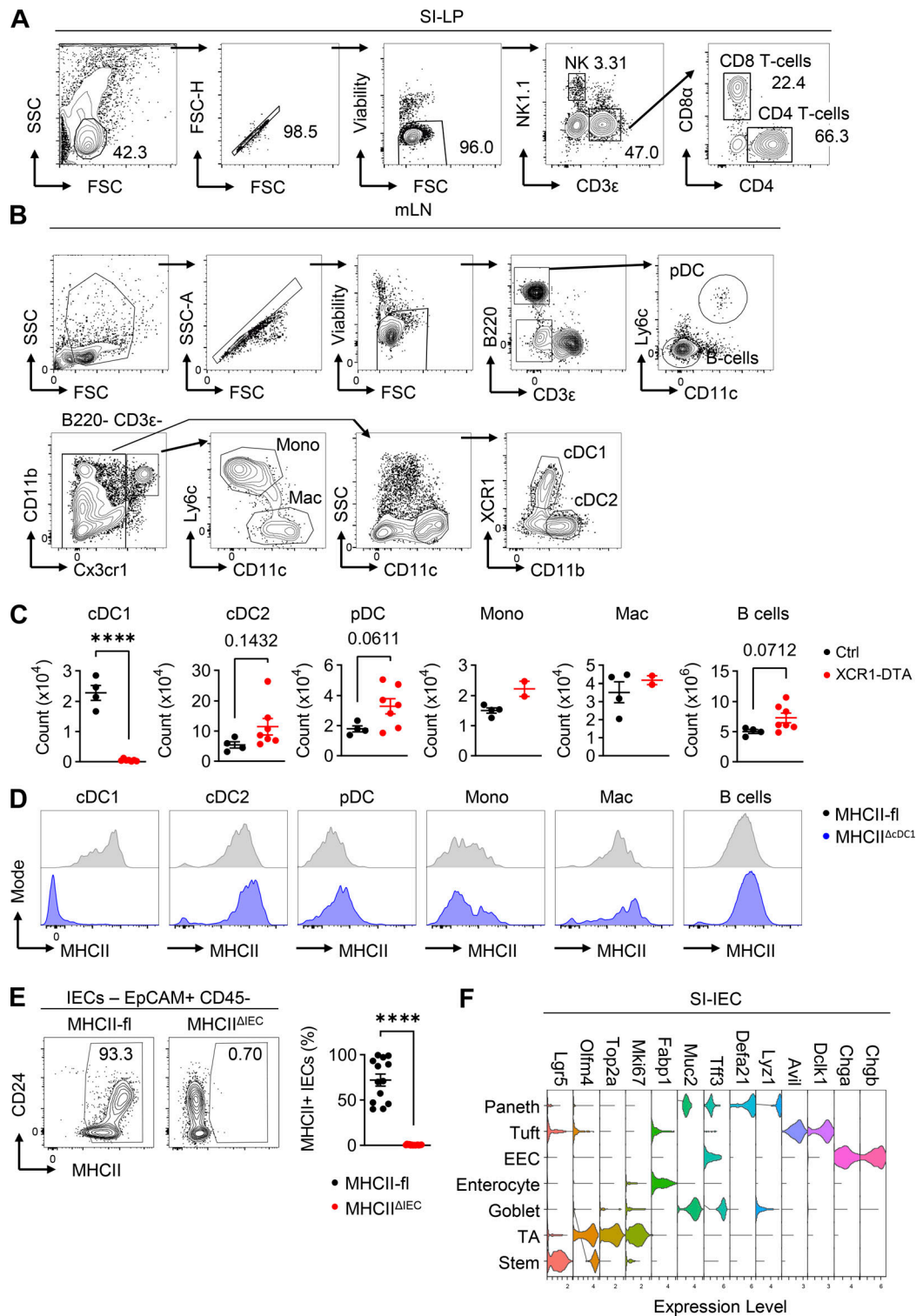


Figure S2. **Representative FACS gating on IFN γ expression analysis, cell-specific targeting validation, and scRNA-seq analysis of SI-IEC from JAX and JAX + SFB mice.** (A) Representative gating used for the analysis of IFN γ expression in NK cells, CD4 and CD8 T cells from SI-LP of loxp-STOP-loxp-Ifng (IFN γ ^{OFF}) and their littermates crossed to Cd4-Cre (IFN γ ^{CD4-ON}) or Ncr1-Cre (IFN γ ^{Ncr1-ON}). Numbers beside gates represent frequency from parent population. (B) Representative gating of mLN APCs. (C) FACS-based quantification of mLN APCs populations from XCR1-DTA mice and their Cre-negative littermates (Ctrl) gated as shown in B. Data are shown as counts. Two independent experiments, $n = 4-7$. (D) FACS-based quantification of MHCII expression in mLN APCs populations from MHCII^{ΔcDC1} mice and their Cre-negative littermates (MHCII-fl) gated as shown in B. (E) FACS analysis of SI-IECs isolated from MHCII^{ΔIEC} mice and their Cre-negative littermates (MHCII-fl). FACS plots on the left show representative gating. Plot on the right shows an overview of the results and statistical analysis. Six independent experiments, $n = 13-14$. (F) Violin plot of canonical markers defining the identity of clusters to cell types in scRNA-seq analysis of SI-IECs from JAX and JAX + SFB mice. Data in C and E were tested by Student's t test. ****, $P < 0.0001$; P values >0.05 are shown. Horizontal lines show mean \pm SEM.

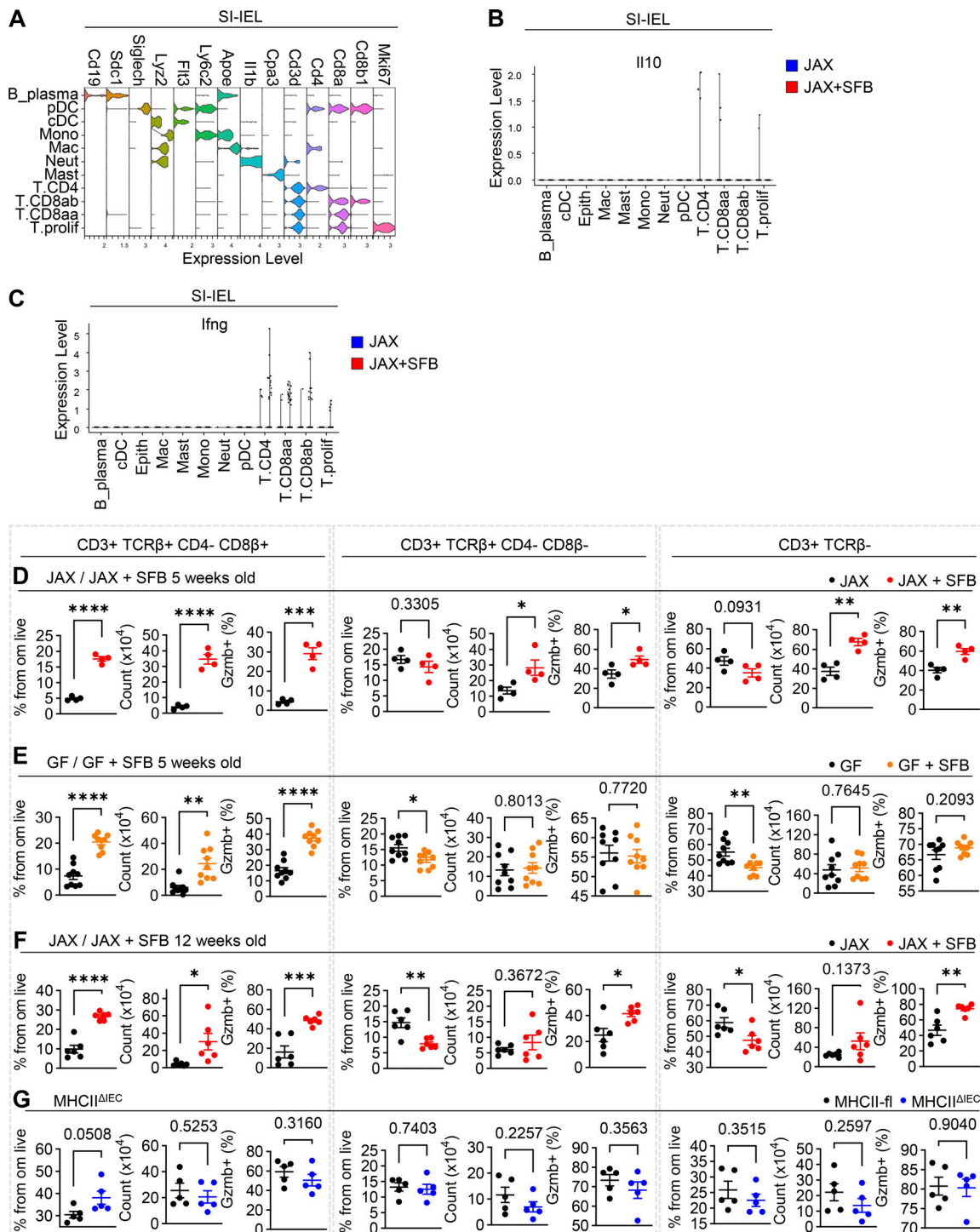


Figure S3. Analysis of SI-IEL after SFB colonization and their dependence on epithelial MHCII. (A) Violin plot of canonic markers defining the identity of clusters to cell types in SI-IEL. We defined several populations of T cells (*Cd3d*): mixed population of proliferating T cells (*Mki67*), CD8a⁺ T cells (*CD8a*, classically termed natural IEL [nIEL]), CD8a^β αβT cells (*Cd8a*, *Cd8b*), and CD4⁺ αβT cells (*Cd4*) (latter two are collectively termed iIEL), which together represented the large majority of analyzed cells. Furthermore, we were able to define several myeloid populations: Mast cells (*Cpa3*), neutrophils (*Il1b*), monocytes (*Ly22*, *Ly6c2*), cDCs (*Flt3*), pDCs (*Siglech*), and macrophages (*Apoe*). We also defined small populations of B/plasma cells (*Cd19*, *Sdc1*). (B) Violin plot of *Ili10* expression in all cell types in SI-IEL separated by their origin from either JAX or JAX + SFB mice. (C) Violin plot of *Ifng* expression in all cell types in SI-IEL separated by their origin from either JAX or JAX + SFB mice. (D-G) FACS analysis IEL compartment. JAX (D and F) or GF (E) animals were colonized by SFB at weaning and analyzed after 2 (D and E) or 9 (F) wk. (G) MHCII^{ΔIEC} mice and their MHCII-fl littermates were injected by tamoxifen at weaning and analyzed after 4 wk. (D-G) For the gating, see Fig. 5. Plots frequencies and counts of respective T cell populations and the frequencies of Gzmb⁺ cell in these population. Two independent experiments, *n* = 4 (D); three independent experiments, *n* = 9 (E); two independent experiments, *n* = 6 (F); two independent experiments, *n* = 5 (G). All data were tested by Student's *t* test. *, *P* < 0.05; **, *P* < 0.01; ***, *P* < 0.001; ****, *P* < 0.0001; *P* values > 0.05 are shown. Horizontal lines show mean ± SEM.

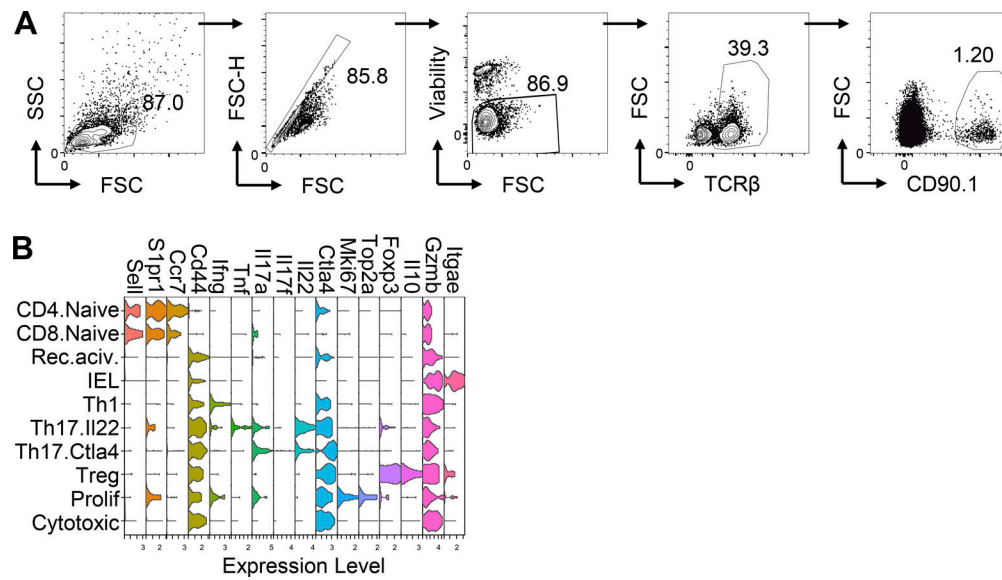


Figure S4. **Analysis of SFB-specific T cell response in SI.** **(A)** Representative gating of adoptively transferred SFBtg T cells in the recipient mice based on CD90.1 congenic marker. Numbers beside gates represent frequencies. **(B)** Violin plot of canonic markers defining the identity of clusters to cell types in SI-LP and SI-IEL cells of mice which received adoptive transfer of SFBtg T cells.

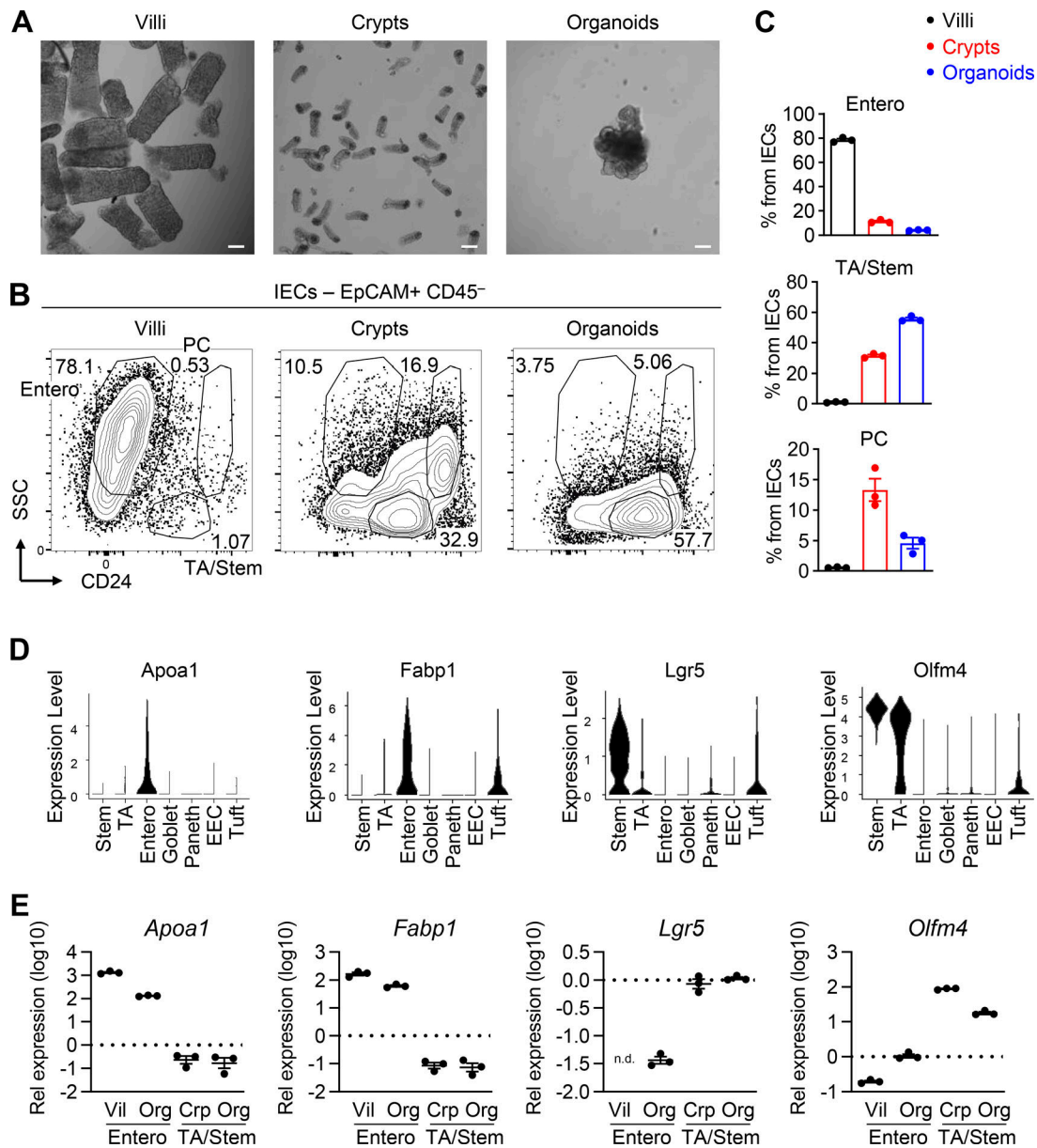


Figure S5. **Establishment of flow cytometry-based analysis of enterocytes.** Intestinal organoids were established as described in Fig. 7 without the addition of IFN γ or IELs. On day 7 of culture, organoids were harvested, and at the same time, SI crypts and villi were isolated. **(A)** Representative microscopic images of villi, crypts, and organoids. The white line represents 100 μ m scale. **(B)** Representative gating for putative enterocytes and transiently amplifying (TA)/intestinal stem cells (ISC) populations as well as Paneth cells. **(C)** Quantification of frequencies of populations defined in B in crypts, villi, and organoids. Note the enrichment of putative enterocytes in villi isolation and other two populations in crypts. Representative experiment, $n = 3$. **(D)** Expression of selected enterocyte and TA/ISC marker genes across all defined population from scRNA-seq analysis (clustering shown in Fig. 4). **(E)** qRT-PCR analysis of selected enterocyte and TA/ISC marker genes in putative enterocyte and TA/ISC population FACS-sorted from villi, crypts, and organoids, confirming the cellular identity of gated populations. Data are shown as log₁₀ of expression relative to *Casc3* house-keeping gene. Numbers beside gates show frequencies. Representative experiment, $n = 3$ (C and E). Vertical lines show mean \pm SEM.